http://dx.doi.org/10.62762/TEPNS.2026.299860

RESEARCH ARTICLE

Coordinated Integration of Electric Vehicles and Photovoltaic Generation in Radial Distribution Networks: Technical Impacts, Flexibility, and Hosting Capacity

Rupali Brahmachary[1,*], **Ahmet Teke**[2], **Aleksa Babic**[3] and **Zoran Miljanić**[4,5]

[1] Department of Electrical Engineering, National Institute of Technology Durgapur, Durgapur 713209, India
[2] Çukurova University, Adana 01330, Türkiye
[3] Western Area Power Administration (WAPA), Phoenix, AZ 85009, United States
[4] Faculty of Electrical Engineering, University of Montenegro, Podgorica 81000, Montenegro
[5] Refleksing LLC, Podgorica, Montenegro

Abstract

The growth of residential electric vehicle (EV) charging and rooftop photovoltaic (PV) generation is changing the operating conditions of radial distribution feeders: evening charging increases the loading of the distribution transformer and conductors, whereas midday PV export raises voltages and can reverse the power flow. Because these effects occur at different times of day, they are usually studied separately, and the way in which a measure aimed at one problem affects the other is insufficiently documented. This paper proposes a coordinated assessment methodology that combines stochastic EV charging, PV generation, a time-series load flow, PV inverter Volt/VAr control, transformer thermal aging, reliability indicators and hosting-capacity evaluation in one framework. Four charging and storage strategies are compared: unmanaged charging, time-of-use (TOU) response, coordinated charging with vehicle-to-grid (V2G) support, and coordinated charging complemented by a feeder-level battery energy storage system (BESS). Volt/VAr control of PV inverters is assessed separately. The methodology is demonstrated on a representative 0.4 kV low-voltage feeder supplied from a 12.47 kV network. The results indicate that unmanaged charging is the dominant cause of transformer overloading and accelerated insulation aging, that reactive-power control reduces but does not eliminate PV-induced voltage rise, and that coordinated charging, V2G and storage relax the evening loading and midday voltage constraints complementarily, increasing the feeder hosting capacity for EVs and PV. Reliability indicators follow the trend of transformer loading. Practical implications for distribution network operators and the study limitations are discussed.

Submitted: 23 October 2026
Revised: 16 November 2026
Accepted: 21 November 2026
Published: 25 November 2026

Vol. 2, **No.** 4, 2026.
10.62762/TEPNS.2026.299860

***Corresponding author:**
✉ Rupali Brahmachary
brahmachary.rupali29@gmail.com

Citation
Brahmachary, R., Teke, A., Babic, A., & Miljanić, Z. (2026). Coordinated Integration of Electric Vehicles and Photovoltaic Generation in Radial Distribution Networks: Technical Impacts, Flexibility, and Hosting Capacity. *ICCK Transactions on Electric Power Networks and Systems*, 2(4), 175–203.

© 2026 by the Authors. Published by Institute of Central Computation and Knowledge. This is an open access article under the CC BY license (https://creativecommons.org/licenses/by/4.0/).

Keywords: electric vehicle (EV), hosting capacity, photovoltaic (PV) system, vehicle-to-grid (V2G) system, Volt/VAr control, transformer aging.

1 Introduction

Distribution networks have traditionally been designed to supply load from substations using radial feeders. Because of this design, equipment ratings, voltage control settings and protection schemes have been set based on load demand being supplied one way from the substation [1, 2]. The rise of electric vehicles (EVs) and the widespread adoption of distributed photovoltaic (PV) systems are, however, set to alter the operating dynamics of such radial distribution networks. The introduction of high-capacity EV chargers and customer-side power generation means these traditional methods are no longer optimal. Feeders might encounter increased demand from EVs, and PV generation could subsequently decrease this load or contribute power to the feeder. In particular, uncontrolled EV charging results in a heightened evening peak load for the distribution system, causing accelerated aging of distribution transformers and reduced voltages at the far ends of feeders. During midday, increased PV output often triggers back-feeding and causes voltage to exceed normal operating parameters. Although these effects occur at different times of day, they act on the same transformer and conductors, and they therefore demand a unified assessment rather than isolated consideration.

Grid effects due to EV charging are dependent on several factors including number of vehicles, charger rating, time of arrival/departure, amount of energy needed, charging coincident factor and where the chargers are located. Residential charging is expected to take place mainly when people arrive home from work, a period that frequently overlaps with standard home energy demands. Prior research suggests this trend results in elevated feeder loads and losses, as well as poorer voltage profiles [3–5]. This is more significant if the transformer and low-voltage conductors were designed for conventional residential demand that did not include EV charging. Charging infrastructure creates a distinct planning concern, because the charger power and the interface to the utility determine the load that the feeder has to supply [6, 7], and because the location of charging stations has to be coordinated with network expansion planning and forecast load growth [8].

PV injection leads to similar issues. If there is more local production than local demand, then there could be a flow of active power towards the substation and cause higher voltages on far nodes of the feeder. The effects of distributed resources and of PV integration on feeder voltage have been summarised in [9, 10], and reactive-power control by inverters, alongside active-power reduction, offers a solution to these challenges [11, 12]. The presence of distributed generation leads to fluctuating fault current levels and orientations, prompting a potential overhaul of protection configurations to adhere to interconnection demands [9, 13, 14]. The variability of solar irradiance causes voltage fluctuations on the feeder [15], and rooftop PV changes the net feeder loading in a way that distributed storage can help to mitigate [16]. The options for controlling the reactive power of distributed PV inverters to limit the voltage rise have also been compared by Turitsyn et al. [17].

A key feature is the mismatch between typical PV production and residential EV charging. PV generation is generally greatest around midday [16], whereas unmanaged residential charging is often greatest in the evening [4, 5, 18]. Consequently, the feeder may experience reverse power flow during the day and high forward loading at night. This complementarity also creates a flexibility opportunity: charging can be shifted toward periods of surplus PV output, and bidirectional EVs or stationary battery energy storage systems (BESS) can provide support during the evening peak. However, the benefits depend on network constraints, customer mobility requirements, communications availability, and the control strategy adopted.

Recent reviews have emphasised the need to assess EV and PV hosting capacity using voltage, thermal, and other operational limits, while accounting for the uncertainty associated with customer behaviour and renewable output [19–21]. Deterministic studies remain useful for screening, but time-series and stochastic methods are better suited to representing coincident peaks and variability. A further challenge is methodological comparability: numerical findings from different networks cannot be compared directly when their feeder parameters, EV profiles, PV assumptions, and constraint definitions differ.

Regarding the impact of EV charging, early assessments of plug-in hybrid and electric vehicle integration established that the timing of charging, rather than the energy consumed, determines the stress placed on distribution assets. Clement-Nyns

et al. [4] showed on a residential feeder that uncoordinated charging increases power losses and voltage deviations, and that optimised charging profiles reduce both. Shafiee et al. [3] and Taylor et al. [5] examined further feeders and penetration levels and likewise reported loading problems for transformers and low-voltage conductors that had been designed for conventional residential demand. These studies are valuable for identifying the mechanisms, but they were carried out without distributed generation and, in general, express the effect on the transformer through its loading ratio without translating overloads into insulation aging. The reviews in [6, 7, 21] confirm that the outcome depends on charger rating, coincidence of arrival times and network characteristics, which limits the transferability of numerical results from one feeder to another.

Various coordination strategies have been proposed at several levels. Sortomme et al. [18] formulated coordinated charging as a loss-minimising quadratic programme, Deilami et al. [22] introduced real-time coordination that uses voltage sensitivities to reduce losses and improve the voltage profile, Sundström and Binding [23] embedded distribution-grid constraints in a flexible charging optimisation, and Ma et al. [24] developed a decentralised valley-filling scheme for large vehicle populations. The common limitation of these approaches is that the objective is formulated for the charging problem alone: PV generation is not considered, the benefit is expressed as reduced losses or a flatter load rather than as transformer life or hosting capacity, and the decentralised scheme in [24] does not explicitly enforce network constraints. Price-based incentives are a simpler alternative, but a uniform low tariff can synchronise charging at the start of the low-price period and create a new peak.

The consequences of overloading for the transformer are quantified with the loading guides IEC 60076-7 and IEEE C57.91 [25, 26]. Staszewski and Rebizant [27] compared the overload risk predicted by the two guides, which indicates that loss-of-life results depend on the guide and on the parameter set adopted. Loss-of-life values are nevertheless often reported without the reference life and thermal parameters needed to interpret them, which weakens the comparison between studies. Fernández et al. [28] assessed the effect of plug-in electric vehicles on the investment costs and energy losses of distribution networks, which include the reinforcement of overloaded transformers and lines, and found that both depend on the charging strategy; this links transformer loading to network losses and to the cost of reinforcement. Further, Walling et al. [9] summarised the effect of distributed resources on feeder voltage, losses and protection, and Katiraei and Agüero [10] discussed the integration challenges specific to PV. On feeders with a high resistance, the voltage rise caused by active-power export is the dominant PV-related constraint. Two families of remedies have been studied. Jahangiri and Aliprantis [11] used distributed Volt/VAr control by PV inverters, and Tonkoski et al. [12] proposed coordinated active-power curtailment for overvoltage prevention. Reactive-power control retains the energy yield but is limited by the inverter apparent-power rating and by the high R/X ratio of distribution conductors, whereas curtailment is effective but sacrifices energy.

Kempton and Tomić [29] established the power and revenue fundamentals of V2G, and Habib et al. [6] and Yilmaz and Krein [7] reviewed the implications of V2G for distribution systems and utility interfaces. These works emphasise technical potential and economics rather than feeder-level constraints. Storage and flexible demand have been proposed to absorb PV surplus and to support the evening peak: Alam et al. [16] managed the available capacity of distributed storage to mitigate rooftop PV impacts and support the evening peak, Oudalov et al. [30] sized a battery energy storage system (BESS) for peak shaving, Brooks et al. [31] described demand dispatch as a way of aligning flexible load with supply, and Dunn et al. [32] reviewed the technologies for grid-scale storage. Hashemi and Østergaard [33] proposed a control of distributed energy storage based on voltage sensitivity that prevents overvoltage and increases the PV hosting capacity of low-voltage grids. In these studies the storage or flexible demand is treated separately from EV charging dynamics, and transformer aging and reliability are generally not evaluated.

Hosting capacity provides a common framework for quantifying how much new generation or demand can be connected without violating specified operating limits. Umoh et al. [19] reviewed deterministic, time-series, stochastic, optimisation-based and streamlined methods for PV and EV hosting-capacity determination in low-voltage networks, Zenhom et al. [20] reviewed renewable and EV hosting capacity in active distribution networks, and Nutkani et al. [21] summarised EV impacts and mitigation methods. Voltage and thermal limits are among the operating

limits that define hosting capacity, and probabilistic assessments of low-voltage networks with PV and EVs have evaluated both [34]. These reviews indicate that hosting capacity is not a universal percentage: it depends on feeder topology, load and generation profiles, control capabilities and the performance indices selected.

Finally, controlled charging and V2G depend on communication between chargers, aggregators and the network operator. Acharya et al. [35] analysed the cybersecurity of smart EV charging from a power-grid perspective, and Acharya et al. [36] examined whether publicly available charging and grid data could constitute a new attack vector. These studies establish the risk but do not quantify how a loss of flexibility affects feeder loading or reliability indices. Reliability is conventionally assessed with the definitions of IEEE Std 1366 [37] and the analytical methods of [38], but the link between feeder loading and interruption indices is seldom made explicit in EV and PV studies.

Four research gaps are identified from this review. First, EV charging and PV integration are mostly analysed separately, so the interaction between evening charging, midday export and the measures aimed at each of them is rarely evaluated on a common time axis and with a common set of constraints. Second, transformer thermal aging and reliability, which translate loading into lifetime and customer-interruption consequences, are seldom linked to hosting capacity in the same study, and loss-of-life figures are often given without the reference life and thermal parameters needed to interpret them. Third, inverter voltage control is frequently described only qualitatively: the reactive-power limits derived from the applicable interconnection standard (IEEE Std 1547-2018) and the resulting reduction in peak voltage are not always stated. Fourth, the load-flow method, the voltage band, the stochastic assumptions and the criteria that define hosting capacity are often undocumented, which prevents comparison between studies and the reproduction of results.

The main contributions of this work are: (i) a coordinated time-series methodology that evaluates EV charging, PV generation, feeder voltage, transformer aging, reliability and hosting capacity within one feeder model and with a common notation; (ii) an explicit formulation of PV Volt/VAr control constrained by the inverter capability and by the reactive-power limits of IEEE Std 1547-2018, together with a peak-voltage-reduction metric; (iii) a documented description of the simulation procedure and of the unmanaged, TOU, coordinated-charging and V2G algorithms; (iv) a hosting-capacity definition based on explicit voltage, thermal, inverter and storage constraints and on a violation-probability criterion, together with a discussion of the voltage band adopted; and (v) a comparative assessment of mitigation options with a discussion of their implications for distribution network operators, including reliability and cybersecurity aspects.

The remainder of the paper is organised as follows. Section 2 describes the feeder and presents the mathematical formulation of the EV, PV, load-flow, Volt/VAr control, transformer aging, V2G, hosting-capacity and reliability models. Section 3 presents the proposed methodology, including the simulation procedure and the charging and V2G algorithms. Section 4 describes the case study and its parameters. Section 5 presents and discusses the results, including the implications for network operators. Section 6 concludes the paper and indicates directions for future work. Appendix A derives the voltage-change approximation of Eq. (15), Appendix B summarises the state-of-charge formulation, Appendix C gives screening estimates of hosting capacity, Appendix D describes the load-flow algorithm and Appendix E elaborates the objective functions.

2 System Description and Mathematical Formulation

2.1 Feeder representation, voltage level and notation

The system under study is a radial distribution feeder (Figure 1) supplied from a 12.47 kV network through a 500 kVA, 12.47 kV/0.4 kV distribution transformer. The transformer supplies a three-phase secondary feeder that serves 120 residential customers equipped, in varying proportions, with EV chargers and rooftop PV systems. The feeder is represented by the source, the transformer, the line sections and the customer buses; a feeder-level BESS and the communication path to the EV aggregator and distributed energy resource management system (DERMS) are included in the scenarios that use them.

Voltage level of the analysis. The load flow is solved on the secondary (low-voltage) feeder. Voltages are expressed in per unit of its nominal line-to-line voltage, and the 12.47 kV network is represented by an ideal voltage source of 1.00 p.u. at the secondary busbar

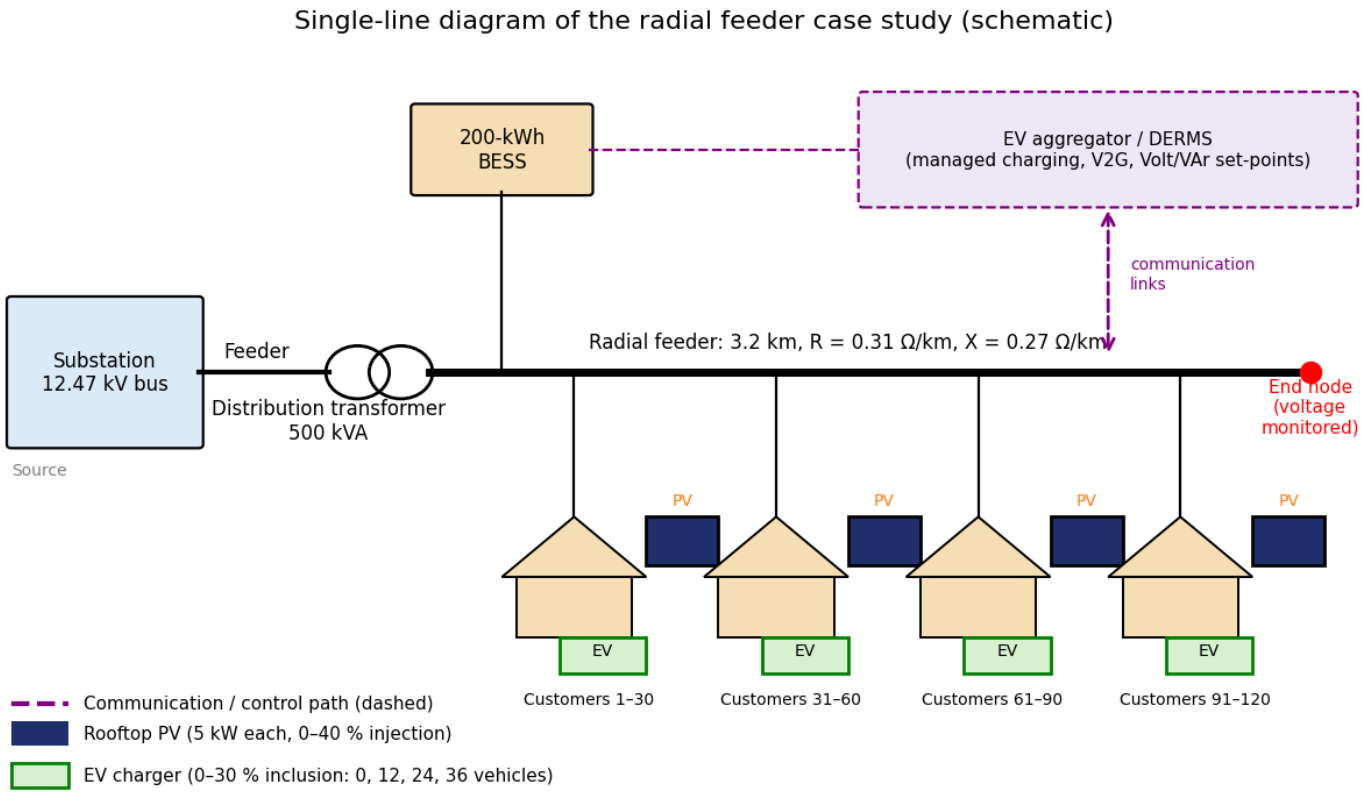


Figure 1. Single-line diagram of the radial distribution feeder used in the case study: 12.47 kV substation, 500 kVA, 12.47 kV/0.4 kV distribution transformer, 0.4 kV low-voltage secondary feeder serving 120 residential customers with rooftop PV and EV chargers, optional 200-kWh battery energy storage system (BESS), and the communication path to the EV aggregator/distributed energy resource management system (DERMS). The grouping of customers is schematic.

of the transformer. The end-node voltage is therefore the voltage at the most remote customer bus of the low-voltage feeder, and the line parameters refer to this feeder.

Balanced operation. The feeder is analysed with a balanced three-phase (single-phase-equivalent) model. The assumption rests on three points: the customers, and with them the EV chargers and PV inverters, are assumed to be distributed equally among the three phases (40 customers per phase); the same stochastic EV and deterministic PV and base-load profiles apply to all phases in expectation; and the aim of the study is to compare the relative effect of mitigation strategies rather than to predict phase-level voltages. The assumption is optimistic for low-voltage feeders with single-phase connections, because an uneven allocation of EV and PV connections increases the voltage rise and drop on the most heavily loaded phase and causes neutral current and voltage unbalance.

The main quantities used in the formulation are the active and reactive power (P and Q) at a bus, the bus voltage (V), the line impedance (resistance R and reactance X), the power for EV charging (P_{EV}), the PV generation (P_{PV}), the rated apparent power of the transformer (S_{rated}), the loading ratio (K), the state of charge (SoC) of a battery, and the minimum and maximum voltage limits ($V_{\min}$ and $V_{\max}$).

2.2 EV charging energy and aggregate demand

The battery energy balance for vehicle i is expressed as [23]

$$E_i \frac{d\,\mathrm{SoC}_i(t)}{dt} = \eta_c P_{EV,i}(t) \tag{1}$$

where E_i is usable battery capacity and η_c is charging efficiency (the definition of the state of charge and its discrete-time form are given in Appendix B). Over a charging interval $[t_0, t_1]$, the energy balance becomes [18]

$$E_i \left[\mathrm{SoC}_i(t_1) - \mathrm{SoC}_i(t_0)\right] = \eta_c \int_{t_0}^{t_1} P_{EV,i}(t)\, dt \tag{2}$$

The aggregate EV charging demand is [18]

$$P_{EV}^{agg}(t) = \sum_{i=1}^{N} P_{EV,i}(t) \tag{3}$$

A diversity factor may be used for screening calculations when only individual peak ratings are available [19]. The diversity factor D_f is defined as the ratio of the sum of the individual maximum demands to the maximum coincident demand of the group [1]:

$$D_f = \frac{\sum_i P_{EV,i,rated}}{P_{EV}^{agg,peak}} \tag{4}$$

With D_f defined in this way, the approximate coincident demand is

$$P_{EV}^{agg,peak} \approx \frac{\sum_i P_{EV,i,rated}}{D_f} \tag{5}$$

This approximation should not be combined with time-series charging profiles that already represent coincidence, since doing so would double-count diversity. The total feeder demand before PV generation [18] is

$$P_{load}(t) = P_{base}(t) + P_{EV}^{agg}(t) \tag{6}$$

For uncertainty analysis, vehicle arrival time, departure time, required energy, and charger rating are sampled from empirical distributions. The arrival time of each vehicle, measured as the delay τ after the start of the arrival window, is described by an exponential density with arrival rate λ_A:

$$f_A(\tau) = \lambda_A \exp\left(-\lambda_A \tau\right), \quad \tau \geq 0 \tag{7}$$

and the daily energy demand is represented by a log-normal distribution, $E_d \sim \mathrm{LogN}(\mu_E, \sigma_E^2)$, that is, $\ln(E_d)$ is normally distributed with mean μ_E and variance σ_E^2, provided that the parameters are fitted to the intended population.

The stochastic EV charging model rests on the following assumptions, and the corresponding parameter values are listed in Table 1. (i) Each EV belongs to one customer, is charged at home on arrival and is independent of the other vehicles. (ii) The arrival time of each vehicle, measured from 17:00, is sampled from the exponential model of Eq. (7) with rate λ_A and truncated at 22:00, which concentrates arrivals in the early evening and reproduces the coincidence of charging with the residential peak. (iii) The daily energy requirement E_d (in kWh) is sampled from the log-normal distribution; with $\mu_E = 3.3$ and $\sigma_E = 0.4$ the median is $\exp(\mu_E) \approx 27$ kWh and the mean is $\exp(\mu_E + \sigma_E^2/2) \approx 29$ kWh. (iv) Charging takes place at the constant charger rating $P_{EV,\max}$ until the requested energy has been delivered, with charging efficiency η_c. (v) The vehicle must have received the requested energy by its departure time, which is 07:00 on the following morning. (vi) EV owners are distributed over the customers, and therefore over the phases, uniformly at random. For each EV inclusion level and scenario, N_{MC} independent daily samples are generated (Section 3.2) and the probability of violating a voltage or thermal constraint is estimated from this ensemble.

2.3 PV generation and net feeder power

A simplified PV power model [39] is expressed as

$$P_{PV}(t) = P_r^{PV} \left[\frac{G(t)}{G_{STC}}\right] \left[1 + \gamma \left(T_{cell}(t) - 25\,^\circ\mathrm{C}\right)\right] \tag{8}$$

where P_r^{PV} is rated PV capacity, $G(t)$ is plane-of-array irradiance, G_{STC} is the irradiance at standard test conditions (STC), 1000 W/m^2, and γ is the temperature coefficient of power (typically negative for crystalline silicon) expressed per degree Celsius. A simplified nominal operating cell temperature (NOCT) approximation [39] is

$$T_{cell}(t) \approx T_{amb}(t) + \left[\frac{G(t)}{800}\right] (\mathrm{NOCT} - 20\,^\circ\mathrm{C}) \tag{9}$$

The net active power imported from the upstream grid [16] is

$$P_{net}(t) = P_{base}(t) + \left(P_{EV}^{agg}(t) - P_{PV}(t)\right) \tag{10}$$

Positive $P_{net}(t)$ denotes net import and negative $P_{net}(t)$ denotes net export under this sign convention. This definition allows EV demand and PV generation to be assessed on a common time axis.

2.4 Load-flow formulation and voltage sensitivity

Feeder voltages are computed with a balanced backward/forward-sweep (BFS) load-flow method [40–42], solved for every time step of the simulated day. The BFS method was selected because it exploits the radial structure of the feeder, converges reliably for the high R/X ratios of distribution lines and avoids the factorisation of a bus admittance matrix, so that the many time-series runs required by the Monte Carlo procedure remain computationally inexpensive. Let k be a bus, j its upstream neighbour, l the line section between them and $D(k)$ the set of sections fed through bus k. The net complex power at bus k is

$$S_k(t) = \left[P_{base,k}(t) + P_{EV,k}(t) - P_{V2G,k}(t) - P_{PV,k}(t)\right] + j\left[Q_{base,k}(t) + Q_{inv,k}(t)\right] \tag{11}$$

where EV charging is a positive load, PV and V2G injections are negative loads, $P_{EV,k}$ and $P_{V2G,k}$ are the sums over the vehicles connected at bus k, and $Q_{inv,k}$ is the reactive power absorbed by the PV inverters at bus k (positive for absorption, negative for injection). EV chargers are assumed to operate at unity power factor. The backward sweep accumulates the section currents from the end of the feeder towards the source,

$$I_l(t) = \left(\frac{S_k(t)}{V_k(t)}\right)^* + \sum_{m \in D(k)} I_m(t) \tag{12}$$

where the asterisk denotes the complex conjugate. The forward sweep then updates the bus voltages from the source towards the end of the feeder,

$$V_k(t) = V_j(t) - Z_l\, I_l(t) \tag{13}$$

with $Z_l = (R + jX)$ multiplied by the section length. The two sweeps are repeated until the largest change of voltage magnitude between two successive iterations ($n-1$ and n) falls below the tolerance ε given in Table 1:

$$\max_k \left| \left|V_k^{(n)}(t)\right| - \left|V_k^{(n-1)}(t)\right| \right| < \varepsilon \tag{14}$$

The load flow is evaluated as a sequence of independent steady-state snapshots at the time resolution Δt. The Volt/VAr control of Section 2.5 is included in the iteration: at each sweep, $Q_{inv,k}$ is updated from the bus voltage of the previous sweep, so that the voltage-dependent control converges together with the load flow.

For a short radial line segment under a balanced approximation, the voltage-magnitude change can also be estimated analytically by [1, 40]

$$\Delta V \approx \frac{RP + XQ}{V} \tag{15}$$

where P and Q are defined consistently as power flowing toward the receiving node. The sign of ΔV depends on the adopted power-flow convention; for downstream load, voltage generally decreases, whereas downstream generation export can produce a rise. For a three-phase system, the corresponding per-phase formulation must include the appropriate voltage and power bases. Equation (15) is a sensitivity approximation used for interpretation and for the first-order estimate in Section 2.5; all voltages reported in Section 5 are obtained from the BFS solution of Eqs. (11)-(14) (Appendix D). The derivation of Eq. (15) is given in Appendix A.

2.5 PV inverter Volt/VAr control

The PV control strategy referred to in Section 5 is Volt/VAr control, in which each inverter absorbs or injects reactive power as a function of the voltage at its point of connection [11, 14]. Reactive-power absorption reduces the voltage rise [11] and is subject to the inverter capability constraint

$$P_{PV}^2(t) + Q_{inv}^2(t) \le S_{inv,rated}^2 \tag{16}$$

where $S_{inv,rated}$ is the rated apparent power of the inverter. The reactive-power set-point follows a piecewise-linear Volt/VAr characteristic,

$$Q_{inv}(V) = \begin{cases} -Q_{\max}, & V \le V_1 \\ -Q_{\max}\dfrac{V_2 - V}{V_2 - V_1}, & V_1 < V < V_2 \\ 0, & V_2 \le V \le V_3 \\ Q_{\max}\dfrac{V - V_3}{V_4 - V_3}, & V_3 < V < V_4 \\ Q_{\max}, & V \ge V_4 \end{cases} \tag{17}$$

where V is the voltage at the point of connection in p.u., $Q_{inv} > 0$ denotes absorption, and $V_1 < V_2 \le V_3 < V_4$ are the characteristic voltages, with a dead band between V_2 and V_3 in which no reactive power is exchanged. In accordance with IEEE Std 1547-2018 [14], the reactive-power capability is limited to a fraction κ of the rated apparent power,

$$Q_{\max} = \kappa\, S_{inv,rated} \tag{18}$$

with $\kappa = 0.44$ for $V_1 = 0.92$, $V_2 = 0.98$, $V_3 = 1.02$ and $V_4 = 1.08$ p.u. Reactive-power priority is assumed: when $P_{PV}^2 + Q_{inv}^2$ would exceed $S_{inv,rated}^2$, the active power is curtailed so that Eq. (16) holds. With $\kappa = 0.44$ this curtailment is at most $1 - \sqrt{1-\kappa^2} \approx 10\%$ of the rated power, and it occurs only at the maximum reactive-power output.

A first-order estimate of the reactive-power requirement for cancelling the resistive voltage-rise component follows directly from Eq. (15). Representing PV export as $P = -P_{PV}$ and inverter reactive-power absorption as $Q = +|Q_{inv}|$ (both defined as power flowing toward the receiving node), the net voltage change becomes $\Delta V \approx (-RP_{PV} + X|Q_{inv}|)/V$. Setting $\Delta V = 0$ gives $X|Q_{inv}| = RP_{PV}$, that is, $|Q_{inv}| \approx |P_{PV}| \times R/X$, when X is non-zero and the approximation is appropriate. For the case-study line ($R/X = 0.31/0.27 \approx 1.15$), full cancellation would require reactive-power absorption larger than the PV active-power output, which the capability limit in Eq. (16) and the limit κ of Eq. (18)

do not allow. If the inverter is rated close to the PV active-power rating, the maximum absorption of $0.44\,S_{inv,rated}$ can cancel at most about $\kappa X/R \approx 38\%$ of the resistive voltage rise at full output, so inverter control can only partly offset the voltage rise.

To quantify the benefit of the control, the peak-voltage reduction is defined as

$$\Delta V_{pk} = \max_{k,t} V_k^{nc}(t) - \max_{k,t} V_k^{vv}(t) \tag{19}$$

where $V_k^{nc}(t)$ and $V_k^{vv}(t)$ are the bus voltages without control and with Volt/VAr control, and the maxima are taken over all buses k and time steps t. The maximum voltage occurs at midday, when PV output is high and the feeder load is low; this is the condition for which Volt/VAr control is most useful, and ΔV_{pk} is therefore the relevant measure of its benefit.

2.6 Transformer thermal aging

Transformer loading is represented by the ratio of apparent load to rated apparent power [25, 26]:

$$K(t) = \frac{S_{load}(t)}{S_{rated}} \tag{20}$$

A simplified steady-state hot-spot estimate, based on the IEEE and IEC transformer loading guides [25–27], is written as:

$$\theta_H(t) = \theta_{amb}(t) + \Delta\theta_{TO}\left[\frac{1 + r\,K(t)^2}{1 + r}\right]^n + \Delta\theta_H\,K(t)^{2m} \tag{21}$$

where $\theta_H(t)$ is the transformer winding hot-spot temperature (°C), $\theta_{amb}(t)$ is the ambient temperature (°C), $\Delta\theta_{TO}$ is the transformer top-oil temperature rise over ambient at rated load (K), $\Delta\theta_H$ is the hot-spot-to-top-oil temperature gradient at rated load (K), r is the ratio of transformer load loss at rated transformer load to no-load loss, $K(t)$ is the loading ratio of Eq. (20), and n and m are the transformer oil and winding exponents. The top-oil term is written in the form used by the guides, in which the no-load loss contributes to the top-oil rise even at zero load. The exponents and rated temperature rises depend on transformer design and cooling class; the values used are given in Table 1. For time-varying conditions, IEC and IEEE loading models include thermal time constants and the history of transformer top-oil and winding temperatures. Equation (21) is evaluated at every time step as a steady-state estimate, which neglects the thermal inertia of the oil and therefore overestimates the temperature during short peaks; it is thus a simplified and conservative representation rather than a complete dynamic thermal model.

The relative aging acceleration factor is estimated with an Arrhenius-type expression [27], in which 110 °C (383 K) is the reference hot-spot temperature for thermally upgraded paper and 15 000 K is the aging constant:

$$F_{AA}(t) = \exp\left\{\frac{15000}{383} - \frac{15000}{\theta_H(t) + 273}\right\} \tag{22}$$

The equivalent aging over a study period T can be expressed as

$$F_{EQA} = \frac{\int_0^T F_{AA}(t)\,dt}{T} \tag{23}$$

and the loss of insulation life over the study period, as a percentage of the reference insulation life, is

$$LoL = \frac{F_{EQA}\,T}{L_{ref}} \times 100\% \tag{24}$$

where L_{ref} is the normal insulation life at the reference hot-spot temperature, expressed in hours (Table 1). For the daily values reported in Section 5, $T = 24$ h. The reported loss-of-life values are therefore the percentage of the reference insulation life consumed in one day, not an aging factor. Equation (23) is preferable to extrapolating service life from a single peak interval. A reported daily loss-of-life percentage should specify the reference insulation life, the integration interval, the thermal parameters, and whether the percentage refers to equivalent insulation life consumed or an aging factor; these items are stated in Table 1 and in this section.

2.7 Managed charging and V2G constraints

Managed charging can be formulated as a scheduling problem that chooses charging power levels to fulfil each EV's demand before it leaves, while adhering to charger and network constraints [23]. A generic objective is

$$\min\ \alpha \max_t P_{grid}(t) + \beta \sum_t P_{loss}(t)\Delta t + \chi \sum_t C(t) P_{grid}(t)\Delta t \tag{25}$$

where $P_{grid}(t)$ is the active power drawn from the upstream grid (kW), $P_{loss}(t)$ is the feeder active-power loss (kW), $C(t)$ is the time-varying electricity price ($/kWh), and Δt is the time step (h). The first term is the peak grid demand (kW); the second is

the energy lost over the scheduling horizon (kWh, because $P(t)$ is a power quantity and $P(t)\Delta t$ is an energy quantity); and the third is the cost of the energy drawn from the grid (\$). Because the three terms have different units, the weights α, β, and χ also act as unit-conversion factors (for example, α in \$/kW, β in \$/kWh, and χ dimensionless when $C(t)$ is in \$/kWh) and set the relative priority of peak reduction, loss reduction, and charging cost. Alternatively, each term can be normalised by its unmanaged-case value so that the weights are dimensionless. The normalised form, the complete scheduling problem and the effect of the weights are given in Appendix E. The max term is handled by introducing an auxiliary variable $P_{peak} \geq P_{grid}(t)$ for all t and minimising P_{peak}. The objective may be extended to include voltage deviation, transformer aging, renewable curtailment, and battery degradation. For each vehicle,

$$0 \leq P_{EV,i}(t) \leq P_{EV,i,\max} \tag{26}$$

$$\mathrm{SoC}_{\min,i} \leq \mathrm{SoC}_i(t) \leq \mathrm{SoC}_{\max,i} \tag{27}$$

$$\mathrm{SoC}_i(T_{dep,i}) \geq \mathrm{SoC}_{dep,i} \tag{28}$$

For a vehicle discharging to the grid, the state-of-charge balance becomes

$$E_i \frac{d\,\mathrm{SoC}_i(t)}{dt} = -\frac{P_{V2G,i}(t)}{\eta_d} \tag{29}$$

where $P_{V2G,i}$ is positive when power is delivered from the battery to the grid and η_d is discharge efficiency. The mutual exclusion of charging and discharging and the V2G power limit are expressed with a binary variable $u_i(t)$, which equals 1 when vehicle i discharges:

$$0 \leq P_{V2G,i}(t) \leq u_i(t)\, P_{V2G,\max,i} \tag{30}$$

$$P_{EV,i}(t) \leq (1 - u_i(t))\, P_{EV,i,\max}, \quad u_i(t) \in \{0,1\} \tag{31}$$

where $P_{V2G,\max,i}$ is the discharge power rating of the vehicle (15 kW in the case study). In addition, discharging is permitted only while the state of charge stays above a V2G floor $\mathrm{SoC}_{V2G,\min,i}$, chosen so that the departure requirement of Eq. (28) can still be met by the scheduled charging; this protects the mobility needs of the customer. A V2G schedule must therefore satisfy battery energy, power, departure, availability and cycling-cost constraints. The feeder-level balance is

$$\begin{aligned} &P_{grid}(t) + P_{PV}(t) + P_{V2G}(t) \\ &\quad = P_{base}(t) + P_{charge}(t) + P_{loss}(t) \end{aligned} \tag{32a}$$

where $P_{grid}(t)$ is the active power imported from the upstream grid, $P_{base}(t)$ is the non-EV base load, $P_{PV}(t)$ is the PV generation, $P_{V2G}(t) = \sum_i P_{V2G,i}(t)$ is the aggregate V2G discharge, $P_{charge}(t) = \sum_i P_{EV,i}(t) = P_{EV}^{agg}(t)$ is the aggregate EV charging power, and $P_{loss}(t)$ is the feeder loss. Because $P_{PV}(t)$ and $P_{V2G}(t)$ appear on the supply side, vehicles charged directly from on-site PV generation or supported by V2G discharge are already included in $P_{charge}(t)$ without drawing on $P_{grid}(t)$: the grid supplies only the residual charging demand.

When a BESS is present, its discharging power is added to the left-hand side and its charging power (taken from surplus PV or from the grid) to the right-hand side of Eq. (32a), which gives Eq. (32b):

$$\begin{aligned} &P_{grid}(t) + P_{PV}(t) + P_{V2G}(t) + P_{BESS}^{dis}(t) \\ &= P_{base}(t) + P_{charge}(t) + P_{BESS}^{ch}(t) + P_{loss}(t) \end{aligned} \tag{32b}$$

where $P_{BESS}^{dis}(t) \geq 0$ and $P_{BESS}^{ch}(t) \geq 0$ are the discharging and charging power of the BESS, which are not applied simultaneously and whose state of charge follows Appendix B. Without a BESS, both terms are zero and Eq. (32b) reduces to Eq. (32a).

Equations (32a) and (32b) are aggregate active-power balances and are not DC power-flow models: they retain the loss term, and reactive power is treated separately through Eqs. (15) and (16). For a complete AC representation, the reactive-power balance $Q_{grid}(t) + Q_{inv}(t) = Q_{base}(t) + Q_{loss}(t)$ must also be enforced together with the network equations. Equations (32a) and (32b) should therefore be read as the active-power part of the model; the voltage and reactive-power part is solved jointly with it by the load flow of Eqs. (11)-(14) (Appendix D) whenever voltage constraints are active.

2.8 Voltage limits and hosting-capacity formulation

Hosting capacity is defined here as the maximum EV charging or PV capacity that can be connected while the selected operating constraints remain satisfied [19, 20]. A generic formulation is given below; the objective function and constraints are explained in the paragraph after Eq. (38), and the objective function is elaborated in Appendix E:

$$\max\ H_{EV},\ H_{PV} \tag{33}$$

subject to:

$$V_{\min} \leq V_k(t) \leq V_{\max}, \quad \forall k, t \tag{34}$$

$$S_l(t) \le S_{rated,l}, \quad \forall l, t \tag{35}$$

$$S_{sub}(t) \le S_{rated,sub} \tag{36}$$

$$P_{inv}^2(t) + Q_{inv}^2(t) \le S_{inv,rated}^2 \tag{37}$$

$$\mathrm{SoC}_{\min} \le \mathrm{SoC}_j(t) \le \mathrm{SoC}_{\max} \tag{38}$$

In Eq. (33), H_{EV} and H_{PV} are the EV and PV hosting capacities, expressed here as the share of customers with EV chargers (EV inclusion) and with rooftop PV (PV injection), or equivalently as installed charging and PV capacity in kW. The objective maximises the EV charging load and PV capacity that the feeder can accommodate. When both are maximised at once, they can be combined into a single objective (for example, a weighted sum $w_{EV}H_{EV} + w_{PV}H_{PV}$), explored as a Pareto trade-off, or evaluated one at a time with the other held fixed. The inequality constraints are as follows: Eq. (34) bounds the voltage at every bus k and time step t; Eq. (35) limits the apparent-power flow $S_l(t)$ of each line or cable segment l to its rating; Eq. (36) limits the loading of the substation or distribution transformer; Eq. (37) is the inverter capability limit, the same as Eq. (16), with P_{inv} and Q_{inv} the active and reactive power of each inverter; and Eq. (38) bounds the state of charge of each storage unit or EV battery j. The network quantities V_k, S_l and S_{sub} depend on H_{EV}, H_{PV} and the operating schedule through the power-flow equations of Section 2.4, which act as equality constraints.

Choice of the voltage limits. The limits $V_{\min} = 0.95$ p.u. and $V_{\max} = 1.05$ p.u. are adopted for the low-voltage feeder as a planning band that is tighter than the statutory supply-voltage range. EN 50160 [43] allows a deviation of $\pm 10\%$ from the nominal voltage at the supply terminals of low-voltage customers for 95% of the time, whereas ANSI C84.1 Range A [44] corresponds to approximately $\pm 5\%$ at the service point of low-voltage circuits. The narrower band is retained because the 12.47 kV network and the transformer tap are represented by an ideal 1.00 p.u. source, so that the voltage variation of the medium-voltage (MV) network, the regulation of the transformer and the drop in the customers' internal wiring, none of which is simulated, have to be accommodated in the part of the $\pm 10\%$ range that the feeder does not use; a $\pm 5\%$ limit allocates about half of the band to the feeder and leaves the remainder for these effects. A tighter limit is also customary when the feeder is operated with coordinated control or optimisation, because the control actions are designed to keep the voltages within a narrower window. Since the choice of the limit directly determines the reported hosting capacity, the results in Section 5 are also discussed against the $\pm 10\%$ band.

Because the voltage and flow constraints are nonlinear and the EV and PV profiles are uncertain, hosting capacity is found by an iterative search rather than by a closed-form optimisation (Section 3.5). A penetration level H is accepted when the probability that at least one of the constraints (34)-(38) is violated at some bus, line section or time step does not exceed an accepted value ε_v:

$$P_{viol}(H) = \frac{N_{viol}(H)}{N_{MC}} \tag{39}$$

$$H^* = \max\{H : \; P_{viol}(H) \le \varepsilon_v\} \tag{40}$$

where $N_{viol}(H)$ is the number of Monte Carlo samples (out of N_{MC}) in which at least one of the constraints (34)-(38) is violated, and H^* is the hosting capacity. Optimisation-based alternatives, such as AC optimal power flow with convex or linearised relaxations and metaheuristic searches, are reviewed in [19, 20]. Screening estimates of hosting capacity and the sampling error of the violation probability are given in Appendix C.

Iterative search. The hosting capacity of each strategy is found by the following steps, which are carried out separately for H_{EV} and H_{PV}, with the other quantity held at its base value (Section 3.5).

1. Set the penetration level $H = 0$ and fix the accepted violation probability $\varepsilon_v = 0.05$ and the number of samples $N_{MC} = 120$.
2. Run Algorithm 1 for the level H: draw the N_{MC} samples of the daily EV behaviour, solve the time-series load flow for each sample, and check the constraints (34)-(38) at all buses, line sections and time steps.
3. Count a sample as a violation if any one of the checks fails, and compute $P_{viol}(H) = N_{viol}(H)/N_{MC}$ from Eq. (39).
4. Compare $P_{viol}(H)$ with ε_v. If $P_{viol}(H) \le \varepsilon_v$, accept the level, increase H by 2 percentage points and return to step 2.
5. If $P_{viol}(H) > \varepsilon_v$, stop. The hosting capacity H^* of Eq. (40) is the last accepted level, that is, $H - 2$ percentage points.
6. If no level fails up to the highest simulated level (30% EV inclusion, 40% PV injection), stop there and report the value as a lower bound of the hosting capacity.

Stopping at the first failing level is justified because the transformer and line loading and the voltage rise grow with the penetration, so that the violation probability is expected to increase with H. The search therefore needs no gradient or bracketing information; its resolution is the step of 2 percentage points, and the Monte Carlo sampling error of P_{viol} is given in Appendix C.

Protection coordination, short-circuit duty, power quality, and customer mobility constraints should be included where relevant. Because EV demand and PV output are uncertain, a planning-grade hosting-capacity study should use time-series or probabilistic assessment rather than rely solely on a single deterministic operating point [19, 20].

2.9 Reliability indices

The conventional reliability indices, namely the system average interruption duration index (SAIDI), system average interruption frequency index (SAIFI), customer average interruption duration index (CAIDI) and average energy not supplied (AENS), follow the definitions of IEEE Std 1366 [37] and the analytical series-system method of [38]. For the radial feeder, every failure of a component i (the transformer or a line section) interrupts the N_i customers downstream of it until the component is restored. The failure rate of a component is not taken as constant but is scaled with its loading ratio K_i,

$$\lambda_i = \lambda_{i,0}\, \varphi\,(K_i) \tag{41}$$

where $\lambda_{i,0}$ is the base failure rate (failures per year) and φ is a non-decreasing function of the loading ratio that equals 1 for $K_i \leq 1$ and represents the higher failure probability of overloaded equipment. This is a simplifying assumption, because the relationship between loading and failure is equipment-specific and is not standardised; the base failure rates, restoration times and φ are given in Table 1. With r_i the average restoration time of component i, the indices are

$$\mathrm{SAIDI} = \frac{\sum_i \lambda_i\, r_i\, N_i}{N_T} \tag{42}$$

$$\mathrm{SAIFI} = \frac{\sum_i \lambda_i\, N_i}{N_T} \tag{43}$$

$$\mathrm{CAIDI} = \frac{\mathrm{SAIDI}}{\mathrm{SAIFI}} \tag{44}$$

$$\mathrm{AENS} = \frac{\sum_i \lambda_i\, r_i\, L_i}{N_T} \tag{45}$$

where L_i is the average load interrupted by a failure of component i (kW), and N_T is the total number of customers served. SAIDI is expressed in hours per customer-year, SAIFI in interruptions per customer-year and AENS in kWh per customer-year; $\lambda_i r_i L_i$ is in kWh per year when λ_i is in failures per year, r_i in hours and L_i in kW.

3 Proposed Methodology

3.1 Overview of the framework

The proposed methodology couples the models of Section 2 in the workflow shown in Figure 2. Stage 1 defines the feeder, the scenarios (Section 4) and the parameters of Table 1. Stage 2 generates the inputs: a set of stochastic daily EV profiles obtained by Monte Carlo sampling of the arrival, energy and departure models of Section 2.2, and the deterministic PV, ambient-temperature and base-load profiles of a representative summer day. Stage 3 applies the charging strategy of the scenario (unmanaged charging, TOU response, or coordinated charging with V2G) to obtain the charging and discharging schedules. Stage 4 solves the time-series BFS load flow of Section 2.4, with Volt/VAr control and the BESS where they are present. Stage 5 evaluates the constraints (34)-(38) and the metrics: voltage, loading, peak demand, transformer loss of life and reliability indices. Stage 6 increases the penetration and repeats Stages 2 to 5 until the violation probability exceeds the accepted value, which yields the hosting capacity.

3.2 Simulation procedure

The study uses a hybrid deterministic-stochastic simulation. The base-load, irradiance and ambient-temperature profiles are deterministic and describe one representative day ($T = 24$ h, time step Δt in Table 1), whereas the EV demand is stochastic. For every combination of scenario, EV inclusion level and PV injection level, N_{MC} Monte Carlo samples of the daily EV behaviour are drawn, and each sample is evaluated by a deterministic time-series BFS load flow. The reported quantities (peak transformer loading, end-node voltage, evening peak demand and loss of life) are the means over the samples, and the hosting capacity uses the violation probability of Eq. (39). The results for PV alone, such as the end-node voltage with and without Volt/VAr control, are deterministic, because the PV profile is deterministic and the control is a deterministic function of the voltage. The procedure is summarised in Algorithm 1.

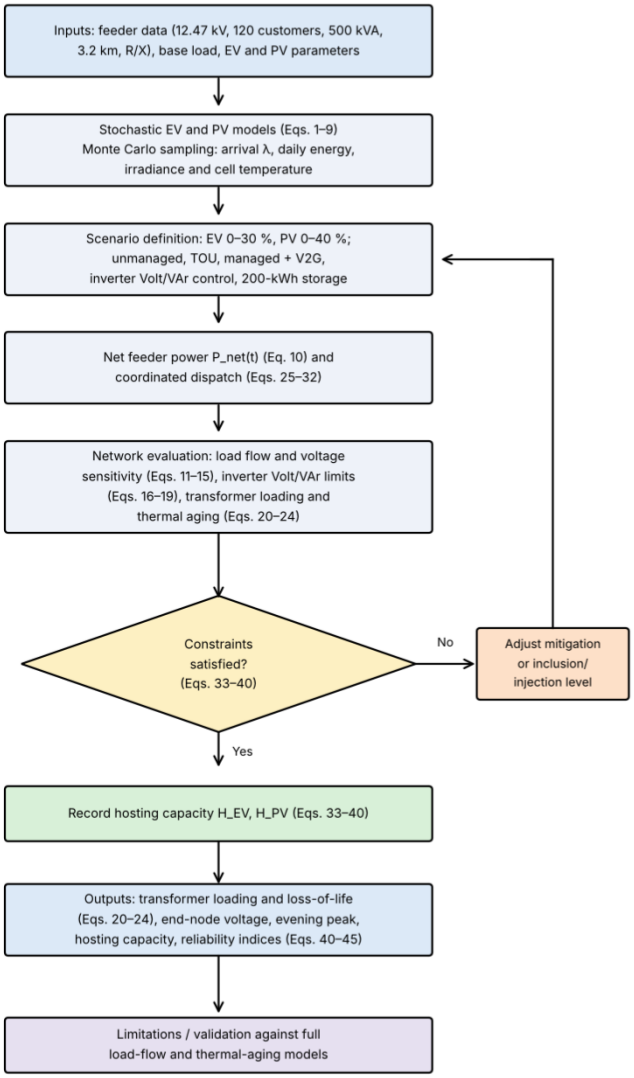


Figure 2. Flowchart of the proposed assessment framework, from input data and stochastic EV/PV models through scenario evaluation and constraint checking to hosting-capacity, loss-of-life and reliability outputs.

Algorithm 1: Time-series assessment of one scenario

Input: feeder data, the parameters of Table 1, the scenario, the EV inclusion level e and the PV injection level p.

Set the sample counter $s = 1$;
repeat
  while $s \leq N_{MC}$ **do**
    Sample the EV fleet: select the customers that own an EV and draw, for each vehicle, the arrival time (Eq. (7)), the energy requirement (log-normal model) and the departure time;
    Generate the vehicle schedules $P_{EV,i}(t)$ and $P_{V2G,i}(t)$ with the charging algorithm of the scenario (Sections 3.3 and 3.4);
    Compute $P_{PV}(t)$ from Eqs. (8) and (9) for the customers with PV;
    foreach *time step* t **do**
      Assemble $S_k(t)$ (Eq. (11)); run the BFS iterations (Eqs. (12)-(14)), updating $Q_{inv,k}$ from Eq. (17) at each sweep when Volt/VAr control is enabled; store $V_k(t)$, $S_l(t)$, $S_{sub}(t)$ and the losses;
    end
    Compute $K(t)$, $\theta_H(t)$, $F_{AA}(t)$ and the loss of life (Eqs. (20)-(24)); check the constraints (34)-(38) and record whether any of them is violated;
    $s \leftarrow s + 1$;
  end
  Compute the sample statistics, the violation probability P_{viol} (Eq. (39)) and the reliability indices (Eqs. (41)-(45)) from the loading ratios;
  Increase e or p by one step and reset $s = 1$;
until $P_{viol} > \varepsilon_v$ (hosting-capacity search, Section 3.5);

3.3 EV charging algorithms

Unmanaged charging. Each vehicle starts charging at the charger rating $P_{EV,\max}$ immediately after arrival and continues for a duration $E_d/(\eta_c P_{EV,\max})$, until the requested energy has been delivered. The aggregate demand follows directly from Eq. (3), and the coincidence of the evening arrivals produces the evening peak.

TOU response. A tariff with a low-price window at midday leads a share $\rho = 60\%$ of the charging energy to be moved into that window, while the remaining 40% is charged on arrival as in the unmanaged case. The shifted energy is spread uniformly over the window and limited by Eq. (26). The behavioural assumption is that the vehicles of the responsive group are available for charging during the window. Because all responsive charging is moved into the same window, a high shifted share can create a new midday peak (a rebound effect) that coincides with the maximum PV output.

Coordinated (managed) charging. An aggregator collects the arrival time, departure time and energy requirement of each plugged-in vehicle and solves the scheduling problem of Eqs. (25)-(28) for the horizon from 17:00 to the latest departure time with the time step Δt. The charging powers enter the

problem linearly; with the voltage expressed through the sensitivity of Eq. (15), the network constraints (34)-(36) are linear as well, so that the problem is a linear programme that is solved once for each Monte Carlo sample. The peak-demand term of Eq. (25) carries the dominant weight, with the loss and cost terms acting as secondary objectives; the auxiliary variable $P_{peak} \geq P_{grid}(t)$ is used for the maximum. The vehicle requirement is met by the departure time through Eq. (28), and the charging windows are therefore spread over the whole period in which the vehicles are plugged in. The aggregator is assumed to know the arrival time and energy requirement of the vehicles within the horizon, which gives an upper bound on the benefit that can be achieved; a rolling-horizon implementation with forecasts would be needed in practice.

3.4 V2G and storage dispatch

A share of the vehicles (the participation share in Table 1) is enrolled as V2G-capable. During the dispatch window from 18:00 to 20:00 the aggregator dispatches discharge of up to $P_{V2G,\max} = 15$ kW per participating vehicle according to the following rule.

(a) At every time step, the net feeder demand without V2G is computed from Eq. (32a) or (32b).

(b) The discharge needed to bring this demand down to the target level, which is the minimum peak found by the scheduling problem, is determined.

(c) This requirement is allocated to the plugged-in participating vehicles in proportion to their energy above the V2G floor, within the limits of Eqs. (29)-(31).

(d) The energy discharged is replaced by charging after the dispatch window and before departure, so that Eq. (28) holds for every vehicle.

The 200-kWh feeder BESS is operated with a rule-based strategy. It charges from the PV surplus when the net feeder power is negative or when the voltage exceeds the upper limit, and from the grid only when its state of charge is lower than the level required for the evening peak. It discharges during the evening peak to reduce the power drawn from the grid. Its power rating and efficiency are given in Table 1, and its state of charge is limited by Eq. (38).

3.5 Hosting-capacity evaluation

Criteria. The EV hosting capacity H_{EV} is the largest EV inclusion (share of customers with an EV charger), and the PV hosting capacity H_{PV} is the largest PV injection (share of customers with a 5 kW rooftop PV system), for which the following criteria are satisfied:

(a) the voltage is within 0.95-1.05 p.u. at every bus and time step, Eq. (34);

(b) the apparent power in every line section is within its rating, Eq. (35);

(c) the transformer loading does not exceed its rating, $K(t) \leq 1.0$ p.u., at any time step, Eq. (36);

(d) the inverter apparent-power limit holds, Eq. (37); and

(e) the state of charge of every storage unit and EV battery stays within its limits, Eq. (38).

A penetration level is accepted when the violation probability of Eq. (39) over the Monte Carlo samples does not exceed ε_v, and the hosting capacity is the largest accepted level, Eq. (40). H_{EV} is evaluated with the PV share held at its base value and H_{PV} with the EV share held at its base value.

Search. The penetration is increased from zero in steps of 2 percentage points, with the number of customers rounded to the nearest whole number (2% of 120 customers is 2.4 customers). At each step, Algorithm 1 is executed, and the search stops at the first level at which the violation probability exceeds ε_v; the hosting capacity is the preceding level. If no violation occurs up to the highest simulated level (30% EV inclusion and 40% PV injection), the reported value is a lower bound of the true hosting capacity.

4 Case Study and Simulation Settings

4.1 Illustrative feeder and scenarios

Base case parameters consist of a 12.47-kV network that supplies, through a 500-kVA distribution transformer, a radial secondary feeder with 120 residential customers (Figure 1). The total feeder length is 3.2 km, with line parameters $R_{line} = 0.31\ \Omega$/km and $X_{line} = 0.27\ \Omega$/km. EV inclusion levels are 0%, 10%, 20% and 30%, or equivalently 0, 12, 24 and 36 vehicles. PV injection levels range from 0% to 40%, where each rooftop PV system is sized at 5 kW.

The EV arrival rate λ_A is specified as 0.8 arrivals per hour, with arrivals between 17:00 and 22:00 (Section 2.2). The daily energy demand of the EVs

Table 1. Parameters and assumptions of the case study.

Parameter	Value	Basis
Network and loads		
Source and transformer	12.47 kV network; 500 kVA, 12.47 kV/0.4 kV transformer; ideal source (1.00 p.u.) at the secondary busbar	Case study
Secondary feeder	Radial; length 3.2 km (1.5-5.0 km in the sensitivity analysis); $R = 0.31\ \Omega$/km, $X = 0.27\ \Omega$/km	Case study
Customers	120, divided equally among the three phases (40 per phase)	Case study
Base load	Residential profile; base peak 353 kW (about 71% of the transformer rating)	Case study
Time resolution, tolerance	$\Delta t = 15$ min, $T = 24$ h; load-flow tolerance $\varepsilon = 10^{-6}$ p.u.	Assumed
PV generation and inverter		
PV systems	5 kW per rooftop system; PV injection 0-40% of customers	Case study
Irradiance, temperature	Representative summer day; peak irradiance 950 W/m^2; ambient temperature 28 °C	Case study
Cell-temperature model	Cell temperature ≈ 52 °C at peak, which corresponds to NOCT ≈ 40 °C in Eq. (9); $\gamma = -0.004\ ^\circ\mathrm{C}^{-1}$	Derived
Inverter and Volt/VAr control	$S_{inv,rated} = 1.0 \times P_r^{PV}$; $\kappa = 0.44$ (IEEE Std 1547-2018 Category B); breakpoints V_1 to V_4 = 0.92, 0.98, 1.02, 1.08 p.u.; reactive-power priority	Standard [14]
EV charging model		
EV inclusion	0, 10, 20, 30% (0, 12, 24, 36 vehicles); steps of 2 percentage points in the hosting-capacity search	Case study
Arrival time	Exponential from 17:00, $\lambda_A = 0.8\ \mathrm{h}^{-1}$, truncated at 22:00	Case study
Daily energy	$E_d \sim \mathrm{LogN}(3.3, 0.4^2)$ in kWh (median ≈ 27 kWh, mean ≈ 29 kWh)	Case study
Battery and charger	Usable capacity 60 kWh; $P_{EV,\max} = 7.2$ kW; $\eta_c = \eta_d = 0.95$; SoC limits 0.10-0.95; departure 07:00	Assumed
Monte Carlo	$N_{MC} = 120$ daily samples per case; accepted violation probability $\varepsilon_v = 0.05$	Assumed
Mitigation options and limits		
TOU response	60% of the charging energy shifted to a midday window of 11:00-15:00	Case study; window assumed
Coordinated charging	Linear programme of Eqs. (25)-(28) and (34)-(36); weights (α, β, χ) = (0.4, 0.2, 0.6)	Assumed
V2G	15 kW per participating vehicle, 18:00-20:00; participation share 60%; SoC floor 0.30	Case study; assumed
BESS	200 kWh; power rating 50 kW; round-trip efficiency 90%; SoC limits 0.15-0.95	Case study; assumed
Voltage limits	0.95-1.05 p.u. (planning band); 0.90-1.10 p.u. used as a sensitivity band	Case study [43, 44]
Transformer aging and reliability		
Thermal parameters	$\theta_{amb} = 28$ °C; $\Delta\theta_{TO} = 55$ K; $\Delta\theta_H = 25$ K; $r = 5$; $n = 0.8$; $m = 1.6$	Typical values [25, 26]
Reference life	$L_{ref} = 0.005$ h at the 110 °C reference hot-spot temperature	Assumed

follows a log-normal distribution with $\mu_E = 3.3$ and $\sigma_E = 0.4$, with E_d in kWh and the natural logarithm, which gives a median of about 27 kWh. PV output is calculated using a representative summer irradiance profile with a peak of 950 W/m^2 and an ambient temperature of 28 °C; the cell temperature

approaches 52 °C, which corresponds to NOCT ≈ 40 °C in Eq. (9). All parameters, with an indication of whether they were taken from the case study, derived from it, or assumed, are collected in Table 1. Each simulation covers one representative 24-hour day with a 15-minute time step (96 time steps per day); the results are therefore daily values and not multi-day or annual statistics.

The cases compared are:

1. Unmanaged EV charging;
2. Managed charging that distributes demand across a broader time window;
3. TOU response shifting 60% of charging toward midday;
4. Managed charging combined with V2G discharge of 15 kW per participating vehicle between 18:00 and 20:00;
5. PV inverter Volt/VAr control with the reactive-power limits of IEEE Std 1547-2018; and
6. Managed charging combined with a 200-kWh feeder BESS.

4.2 Simulation settings

The results shown below are derived from applying the proposed methodology (Section 3 and Algorithm 1) to the case study. Feeder loading, voltage variations, transformer thermal loading, coordinated charging, V2G and inverter-based voltage regulation are evaluated. A comparative analysis of the results is undertaken to examine the effects of the mitigation techniques discussed, their efficacy, and their implications for the flexibility of the distribution network and its capacity to accommodate new loads. The numerical findings are interpreted within the assumptions and limitations of the case study.

5 Results and Discussion

5.1 Transformer loading and reported insulation-life consumption

Table 2 and Figure 3 show that the peak transformer loading increases from 71% of rated for baseline conditions to 113% of rated at 30% EV inclusion for unmanaged charging. The latter is above the 500-kVA rating of the existing distribution transformer and essentially means that some type of intervention (either reinforcement or demand management) would be required to accommodate the EV load if left to charge without management. Peak loading with managed charging for this same inclusion level is estimated to be 88%, which is a reduction of 25 percentage points compared to the unmanaged case. The daily loss of life in Table 2 is calculated with Eqs. (20)-(24) and the parameters of Table 1.

Table 2. Peak transformer loading and reported daily loss-of-life for different EV inclusion levels and charging modes.

EV inclusion	Charging mode	Peak transformer loading	Reported daily loss-of-life
0%	Unmanaged	71%	0.27%
10%	Unmanaged	84%	0.61%
20%	Unmanaged	97%	1.34%
30%	Unmanaged	113%	3.82%
10%	Managed	78%	0.41%
20%	Managed	86%	0.69%
30%	Managed	88%	0.74%

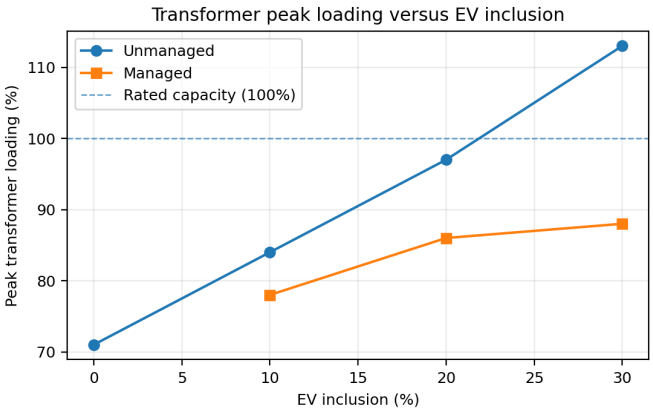


Figure 3. Transformer peak loading versus EV inclusion for unmanaged and managed charging, with the 100% rated capacity shown for reference.

The reported daily loss-of-life value (percentage of the reference insulation life consumed per day, Eq. (24)) decreases from 3.82% to 0.74% for the same comparison (Figure 4). The percent decrease in the stated metric is about 80.6%. This large reduction shows that the calculated transformer aging is sensitive to the hot-spot temperature, ambient conditions, the transformer's thermal time constants, and the duration of the overload.

Managed charging at 30% EV inclusion reduces peak loading by 25 percentage points. Relative to the unmanaged value, this is a reduction of 22.1% ((25/113) × 100%). Likewise, managed charging moves the transformer from 13 percentage points above its nameplate rating to 12 percentage points

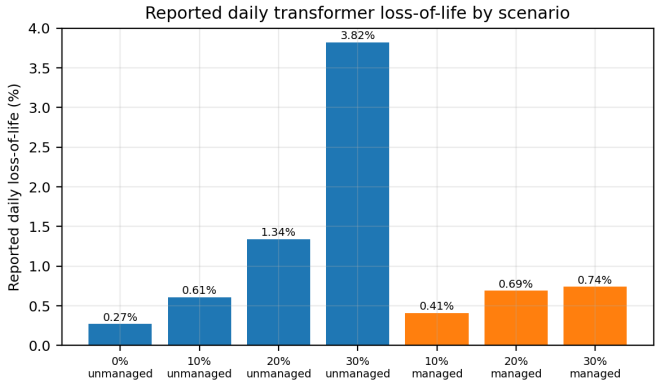


Figure 4. Reported daily transformer loss-of-life (% of insulation life) for unmanaged (blue) and managed (orange) charging at each EV inclusion level.

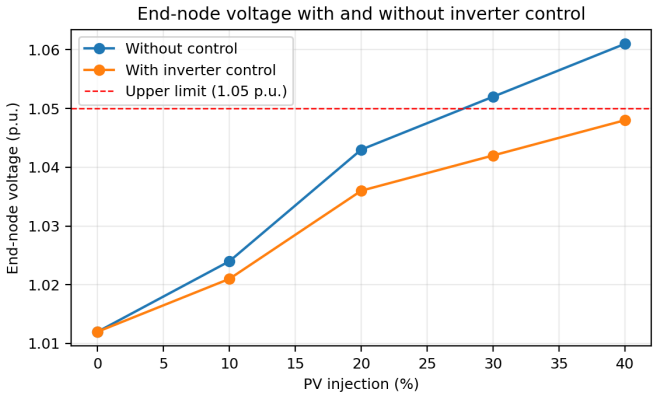


Figure 5. End-node voltage versus PV injection with and without inverter reactive-power control; the dashed line marks the 1.05-p.u. upper voltage limit.

below rating. For comparison at 20% EV inclusion, managed charging reduces the peak by 11 percentage points (Table 3). Such comparisons indicate that the benefit of scheduling increases as coincident EV demand increases, and that load management also reduces the loss of life.

Table 3. Transformer loading reduction achieved by managed charging relative to unmanaged charging.

EV inclusion	Unmanaged loading	Managed loading	Loading reduction	Unmanaged overload above rating
10%	84%	78%	6 percentage points	–
20%	97%	86%	11 percentage points	–
30%	113%	88%	25 percentage points	13 percentage points

5.2 PV injection, end-node voltage and peak-voltage reduction

Table 4 and Figure 5 show that the end-node voltage increases monotonically with PV injection. At 40% injection, the voltage without inverter control exceeds the upper limit of 1.05 p.u., reaching 1.061 p.u. With Volt/VAr control, it reaches at most 1.048 p.u., which shows the benefit of even limited voltage support at the point of common coupling (PCC). The difference of 0.013 p.u. is the peak-voltage reduction ΔV_{pk} of Eq. (19) at this injection level. The voltage without control is greater than 1.05 p.u. at both 30% and 40% PV injection, by 0.002 p.u. and 0.011 p.u., respectively. The values under inverter control are 1.042 and 1.048 p.u., respectively, both below the upper limit.

Peak-voltage reduction. The reduction columns of Table 4 give ΔV_{pk}: it grows with PV injection from 0.003 p.u. at 10% to 0.013 p.u. at 40%, that is, from 0.29% to 1.23% of the uncontrolled voltage. The maximum voltage occurs at the end node at midday, when PV output is highest and the feeder load is low, and this is the condition for which Volt/VAr control is most useful; the reduction at this point is therefore the relevant measure of its benefit. Expressed relative to the voltage rise caused by PV (the difference between the uncontrolled voltage and the 1.012 p.u. obtained without PV), the control removes about 23% to 27% of the rise at the PV levels considered. This is below the first-order upper bound of about 38% derived in Section 2.5 from Eq. (15), the ratio $R/X = 1.15$ and $\kappa = 0.44$. Volt/VAr control is thus limited by the reactive-power capability of the inverters and by the high R/X ratio of the feeder, which is why storage or active-power management is needed at higher PV levels (Section 5.5). The use of battery storage together with PV to support the feeder voltage profile is consistent with the finding of Hashemi and Østergaard [33] that efficient control of storage increases the PV hosting capacity of low-voltage grids by limiting overvoltage.

Voltage band. The upper limit of 1.05 p.u. is a planning limit that is tighter than the $\pm 10\%$ supply-voltage range of EN 50160 [43] (Section 2.8).

5.3 Evening peak demand and flexibility

Relative to unmanaged charging, TOU response reduces the reported evening peak by 86 kW, or approximately 17.7%. Managed charging combined with V2G reduces it by 119 kW, or approximately 24.4%. Compared with the 353-kW base peak, the

Table 4. End-node voltage with and without inverter Volt/VAr control for different PV injection levels.

PV injection	Voltage without control (p.u.)	Voltage with control (p.u.)	Reduction (p.u.)	Reduction (% of uncontrolled value)	Status against 1.05-p.u. upper limit
0%	1.012	1.012	0.000	0.00%	Both within limit
10%	1.024	1.021	0.003	0.29%	Both within limit
20%	1.043	1.036	0.007	0.67%	Both within limit
30%	1.052	1.042	0.010	0.95%	Uncontrolled case exceeds limit
40%	1.061	1.048	0.013	1.23%	Control brings voltage below limit

managed V2G scenario leaves an increase of 15 kW (Table 5). These results illustrate that price-based shifting provides a partial benefit, while coordinated dispatch and bidirectional discharge provide a larger peak reduction.

Table 5. Reported evening peak demand at 20% EV inclusion under different charging strategies.

Scenario at 20% EV inclusion	Reported evening peak	Change from 353-kW base peak
Unmanaged charging	487 kW	+38%
TOU response; 60% shifted to midday	401 kW	+14%
Managed charging with V2G	368 kW	+4%

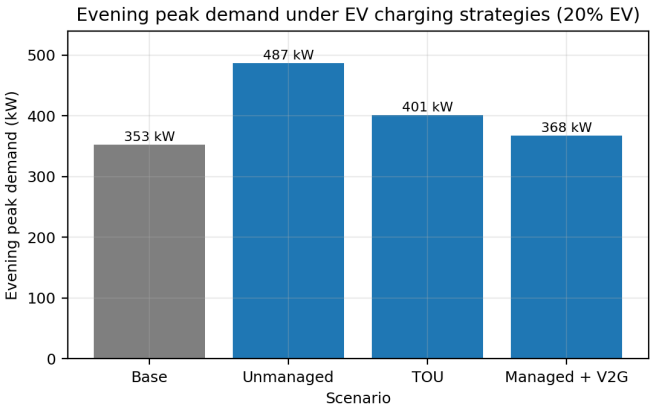


Figure 6. Evening peak demand at 20% EV inclusion under the base case, unmanaged charging, TOU response and managed charging with V2G.

The additional peak load of the unmanaged case is 134 kW above base peak. Subtracting the loads associated with TOU response shows 86 kW of that peak has been avoided by TOU measures (Table 6). Managed charging with V2G gives a total reduction of 119 kW relative to the unmanaged case. Compared to TOU response alone, the improvement from managed-V2G is a further reduction of 33 kW, or 8.2% of the TOU peak. The resulting 368 kW peak is still 4.2% above the base peak, although most of the EV-related increase has been removed (Figure 6).

5.4 Feeder length and charging coincidence

The findings also reveal that as feeder length increases from 1.5 km to 5.0 km, voltage drop at 30% EV inclusion rises from 0.041 p.u. to 0.096 p.u. (Table 7, Figure 7). The drop increases with the line impedance, although less than proportionally to the feeder length, since the average drop per kilometre decreases from 0.0273 to 0.0192 p.u./km. The 5-km case violates the 0.95-p.u. lower voltage limit under unmanaged charging. In addition, a screening estimate based on Eq. (5) illustrates the effect of charging coincidence. For the 36 vehicles of 7.2 kW at 30% EV inclusion and the 353-kW base peak, a coincidence factor $(1/D_f)$ of 1.0 gives a transformer loading of about 122% of rating, and reducing it to 0.6, that is, increasing D_f from 1.0 to about 1.67, reduces the loading to about 102%. The simulated unmanaged value of 113% corresponds to an effective coincidence factor of about 0.82. This illustrates how strongly the transformer result depends on the assumed coincidence of charging.

An increase in feeder length from 1.5 km to 5.0 km resulted in an increase of 0.055 p.u. in the voltage drop, or roughly 134.1% relative to the shorter feeder. Under unmanaged charging, the 5-km scenario falls below the 0.95-p.u. minimum threshold of the planning band: with a 1.00 p.u. source, a drop of 0.096 p.u. gives about 0.904 p.u. at the end of the feeder, which would still be marginally within the $\pm 10\%$ band of EN 50160 [43] but not within the $\pm 5\%$ band.

5.5 Hosting capacity under mitigation scenarios

From Table 8 and Figure 8, the hosting-capacity comparison indicates that demand flexibility primarily increases the permissible EV inclusion, while storage

Table 6. Detailed comparison of evening peak demand against the unmanaged case and the base peak.

Scenario	Peak demand (kW)	Reduction vs. unmanaged (kW)	Reduction vs. unmanaged (%)	Difference from base peak (kW)	Difference from base peak (%)
Base peak	353	–	–	0	0.0%
Unmanaged charging	487	0	0.0%	+134	+38.0%
TOU response (60% shifted to midday)	401	86	17.7%	+48	+13.6%
Managed charging with V2G	368	119	24.4%	+15	+4.2%

Table 7. Reported voltage drop at 30% EV inclusion for different feeder lengths.

Feeder length (km)	Reported voltage drop (p.u.)	Average drop per km (p.u./km)	Change from 1.5-km case
1.5	0.041	0.0273	Reference
5.0	0.096	0.0192	+0.055 p.u. (+134.1%)

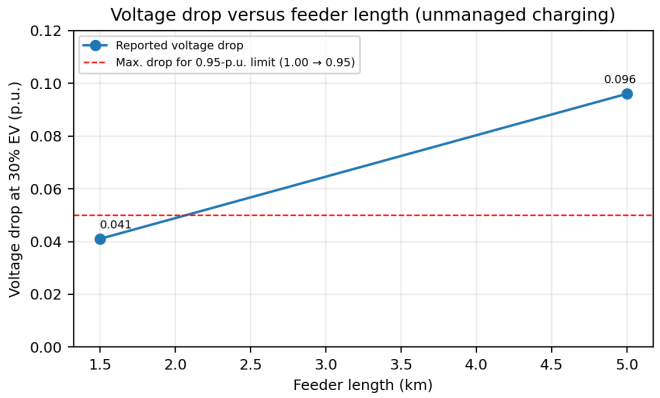


Figure 7. Voltage drop at 30% EV inclusion for 1.5-km and 5.0-km feeders under unmanaged charging; the dashed line shows the drop that would bring a 1.00-p.u. source voltage to the 0.95-p.u. lower limit.

combined with managed charging is associated with the largest PV hosting capacity. In the final scenario, the reported capacities reach 30% EV inclusion and 40% PV injection. Following the criteria of Section 3.5 and Eqs. (33)-(40), each entry of Table 8 is the largest value of H_{EV} or H_{PV} found for the corresponding scenario for which the constraints in Eqs. (34)-(38) (voltage limits, line and transformer loading, inverter capability and storage state of charge) are satisfied, with a violation probability not exceeding ε_v. Demand flexibility (TOU tariffs, managed charging and V2G) mainly relaxes the evening transformer-loading constraint of Eq. (36), which limits H_{EV}, whereas storage mainly relaxes the midday voltage constraint of Eq. (34), which limits H_{PV}. Because the highest EV and PV levels simulated are 30% and 40%, values reported at these levels show that no constraint was violated up to the upper end of the simulated range and should be read as lower bounds of the true hosting capacity.

Compared with no mitigation, TOU tariffs increase reported EV hosting capacity by 6 percentage points (33.3% relative to 18%), but do not change the reported PV hosting capacity. Managed charging with V2G increases EV hosting capacity by 12 percentage points (66.7%) and PV hosting capacity by 6 percentage points (27.3%). Adding 200-kWh storage to managed charging yields the same reported EV capacity as V2G alone but raises PV capacity from 28% to 40%. This pattern is consistent with storage being particularly useful for absorbing midday PV surplus, while EV scheduling and V2G primarily address coincident charging demand.

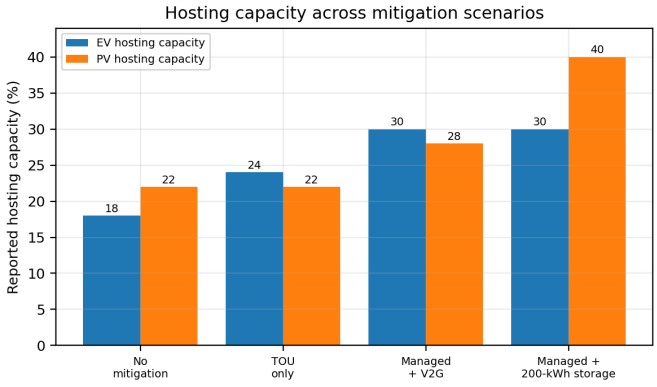


Figure 8. EV and PV hosting capacity across the four mitigation scenarios.

5.6 Reliability indicators

Table 9 shows the reliability indices computed with the method of Section 2.9 at various EV inclusion levels and charging profiles. As expected, SAIDI, SAIFI, and AENS increase with greater amounts of unmanaged EV inclusion. This trend shows that the reliability

Table 8. EV and PV hosting capacity under different mitigation scenarios.

Mitigation scenario	EV hosting capacity	EV gain vs. no mitigation	PV hosting capacity	PV gain vs. no mitigation
No mitigation	18%	0 percentage points	22%	0 percentage points
TOU tariffs only	24%	+6 percentage points	22%	0 percentage points
Managed charging with V2G	30%	+12 percentage points	28%	+6 percentage points
Managed charging + 200-kWh storage	30%	+12 percentage points	40%	+18 percentage points

of the distribution system may degrade with higher loading levels. Comparing the managed charging case at 30% EV inclusion with the unmanaged charging case, managed charging decreases SAIDI, SAIFI, and AENS. Spreading the charging demand over time limits equipment overloading and thereby improves the reliability indices.

From 0% to 30% unmanaged EV inclusion, SAIDI rises from 1.87 to 5.63 h/customer-year (a 201.1% increase), SAIFI rises from 0.75 to 2.25 interruptions/customer-year (200%), and AENS rises from 52 to 162 kWh/customer-year (211.5%). In the 30% managed case, the reported values are approximately 60.5-60.9% lower than the 30% unmanaged values (Table 10, Figure 9 and Figure 10).

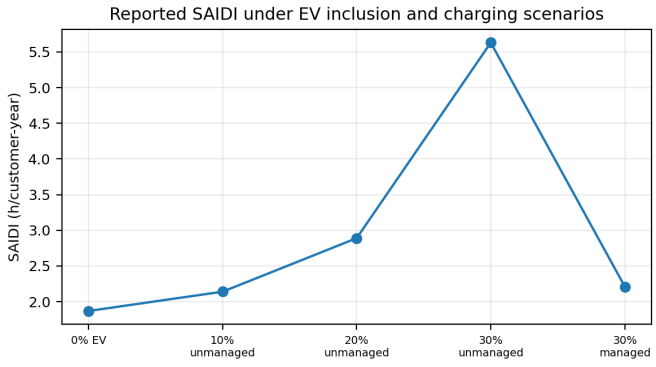


Figure 9. Reported SAIDI under different EV inclusion levels and charging scenarios.

5.7 Cybersecurity and operational dependability

A communication channel arises from the implementation of managed charging, V2G, smart metering, and remote inverter controls. This communication happens via the charging equipment, connecting to either the vehicle or the back-end system, often using standards like International Organization for Standardization (ISO) 15118 and Open Charge Point Protocol (OCPP). Utilities commonly use communication systems such as supervisory control and data acquisition (SCADA) or advanced metering infrastructure (AMI). Threat vectors can vary based on system configuration and design. Attackers may be able to command charging behaviour, gain access to user credentials, disrupt communications or send malicious telemetry. This could cause load to shift at undesirable times and prevent flexibility from being utilised [35, 36].

5.8 Practical implications for distribution network operators

The results have several implications for distribution network operators (DNOs). First, the transformer is the first asset to become critical in the evening: the unmanaged case exceeds the rating at the highest EV inclusion, and the loss-of-life figures show that the consequence grows more than proportionally with the loading. A uniform off-peak tariff alone is not sufficient, because it moves the peak rather than removing it, so that staggered start times or power limits per charger are advisable. Where the rating is exceeded, replacing the transformer with a higher-rated unit is the conventional alternative, and the effect of EV charging on reinforcement investment and network losses has been assessed in [28].

Second, voltage rise is the first PV-related constraint on long feeders with a high R/X ratio. Enabling the Volt/VAr function in the inverter settings at the time of connection, as allowed by IEEE Std 1547-2018, is a low-cost first step, but its effect is limited; feeders that approach their PV hosting capacity will additionally need active-power management [12], storage [16, 33] or conventional network reinforcement, whose investment cost and effect on network losses have been assessed for EV charging in [28].

Third, hosting-capacity figures should be considered together with the criteria behind them (voltage band, thermal limits and accepted violation probability), and values reported at the upper end of the simulated range

Table 9. Reliability indices (SAIDI, SAIFI, AENS) for different EV inclusion levels and charging profiles.

Scenario	SAIDI (h/customer-year)	SAIFI (interruptions/customer-year)	AENS (kWh/customer-year)
0% EV	1.87	0.75	52
10% EV, unmanaged	2.14	0.86	61
20% EV, unmanaged	2.89	1.15	83
30% EV, unmanaged	5.63	2.25	162
30% EV, managed	2.21	0.88	64

Table 10. Reliability improvement with managed charging at 30% EV inclusion.

Metric	0% EV	30% EV unmanaged	30% EV managed	Absolute reduction with management	Relative reduction
SAIDI (h/customer-year)	1.87	5.63	2.21	3.42 h/customer-year	60.7%
SAIFI (interruptions/customer-year)	0.75	2.25	0.88	1.37 interruptions/customer-year	60.9%
AENS (kWh/customer-year)	52	162	64	98 kWh/customer-year	60.5%

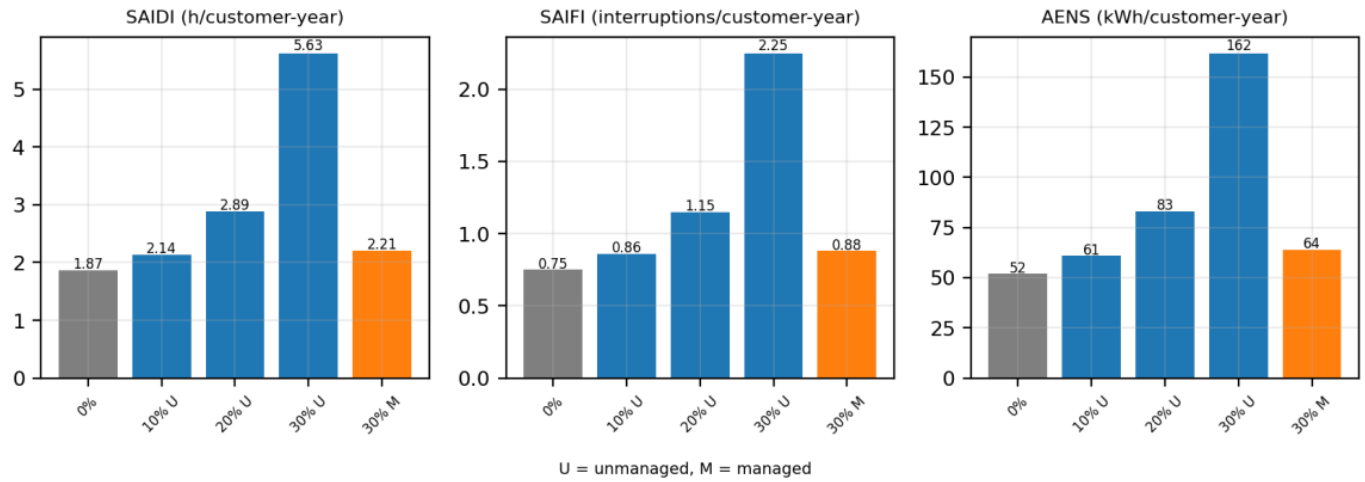


Figure 10. Comparison of reported SAIDI, SAIFI and AENS for the base case (0% EV), unmanaged charging (U) and managed charging (M).

should be treated as lower bounds and updated with measured data.

Fourth, the support provided by V2G and BESS depends on customer participation, on the compensation of battery degradation (not modelled in this study), and on dependable communication. DNOs should therefore specify a safe fallback for the loss of communication, such as local autonomous charging limits and default Volt/VAr settings, because the benefit of coordinated control disappears when commands are lost or manipulated. Finally, since the reliability indicators follow the transformer loading in the case study, loading-based asset monitoring serves as an early-warning indicator.

6 Conclusion

This paper proposed a coordinated methodology to assess the combined impact of residential EV charging and rooftop PV generation on radial distribution feeders. The methodology links a stochastic EV charging model, deterministic PV and base-load profiles, a backward/forward-sweep time-series load flow, PV Volt/VAr control constrained by the inverter capability and the reactive-power limits of IEEE Std 1547-2018, transformer thermal aging, reliability indices and an explicit hosting-capacity criterion. Unmanaged charging, TOU response, coordinated

charging with V2G, and coordinated charging with storage were compared on a representative feeder, and PV inverter Volt/VAr control was assessed separately.

The simulation results lead to the following general conclusions. First, unmanaged charging concentrates demand in the evening, overloads the distribution transformer and accelerates insulation aging, and the damage grows more than proportionally with EV inclusion; coordinated charging largely removes this problem, whereas price-based shifting alone gives only a partial benefit. Second, PV injection raises the end-node voltage, and Volt/VAr control reduces the peak voltage but offsets only part of the rise, because of the reactive-power limits of the inverters and the high R/X ratio of the feeder; storage or active-power management is needed at higher PV levels. Third, because the constraints that limit EV and PV hosting capacity occur at different times of day, they are relaxed by different measures: demand flexibility and V2G for the evening transformer loading, and storage for the midday voltage; combining them gives the largest hosting capacity. Fourth, the reliability indicators follow the trend of transformer loading, so that load management also supports reliability, while the dependence on communication introduces cybersecurity and availability requirements. The voltage band, the load-flow assumptions and the hosting-capacity criteria influence the numerical results and need to be stated in any comparison.

The study is limited by the balanced single-phase-equivalent model, a single representative feeder, and EV and PV parameters that are assumed rather than measured. Future research should employ unbalanced four-wire time-series simulations on a documented benchmark network, calibrated stochastic EV and PV models, validated dynamic thermal-aging models, battery degradation in V2G operation, and an uncertainty-based hosting-capacity assessment that includes communication failures and their effects on network reliability.

Data Availability Statement

Data will be made available on request.

Funding

This work was supported without any funding.

Conflicts of Interest

Ahmet Teke served as an Associate Editor of the *ICCK Transactions on Electric Power Networks and Systems* at the time of manuscript submission. To ensure the integrity and impartiality of the peer-review process, Ahmet Teke was not involved in the editorial handling, peer review, or decision-making for this manuscript, which was handled independently by another editor. Zoran Miljanić is affiliated with Refleksing LLC, Podgorica, Montenegro. This affiliation had no influence on the study design, data collection, analysis, interpretation, or decision to publish. The remaining authors declare no conflicts of interest.

AI Use Statement

The authors declare that no generative AI was used in the preparation of this manuscript.

Ethical Approval and Consent to Participate

Not applicable.

References

[1] Gonen, T. (2014). *Electric power distribution engineering* (3rd ed.). CRC Press. [CrossRef]

[2] Dugan, R. C., McGranaghan, M. F., & Beaty, H. W. (1996). *Electrical power systems quality*. McGraw-Hill. https://www.accessengineeringlibrary.com/binary/mheaeworks/773fbf0510c9c305/128c9e3c6268f565edd4e5546c092bb28282a44c1b99ff5b731e062770c52d54/book-summary.pdf

[3] Shafiee, S., Fotuhi-Firuzabad, M., & Rastegar, M. (2013). Investigating the impacts of plug-in hybrid electric vehicles on power distribution systems. *IEEE Transactions on Smart Grid, 4*(3), 1351-1360. [CrossRef]

[4] Clement-Nyns, K., Haesen, E., & Driesen, J. (2010). The impact of charging plug-in hybrid electric vehicles on a residential distribution grid. *IEEE Transactions on Power Systems, 25*(1), 371-380. [CrossRef]

[5] Taylor, J., Maitra, A., Alexander, M., Brooks, D., & Duvall, M. (2010, July). Evaluations of plug-in electric vehicle distribution system impacts. In *IEEE PES General Meeting* (pp. 1-6). IEEE. [CrossRef]

[6] Habib, S., Kamran, M., & Rashid, U. (2015). Impact analysis of vehicle-to-grid technology and charging strategies of electric vehicles on distribution networks - a review. *Journal of Power Sources, 277*, 205-214. [CrossRef]

[7] Yilmaz, M., & Krein, P. T. (2013). Review of the impact of vehicle-to-grid technologies on distribution systems and utility interfaces. *IEEE Transactions on Power Electronics, 28*(12), 5673-5689. [CrossRef]

[8] Brahmachary, R., & Ahmed, I. (2025). Optimal

distribution network expansion and EV charging station allocation based on load forecasted using machine learning. *IEEE Transactions on Industry Applications, 61*(4), 5699-5713. [CrossRef]

[9] Walling, R. A., Saint, R., Dugan, R. C., Burke, J., & Kojovic, L. A. (2008). Summary of distributed resources impact on power delivery systems. *IEEE Transactions on Power Delivery, 23*(3), 1636-1644. [CrossRef]

[10] Katiraei, F., & Agüero, J. R. (2011). Solar PV integration challenges. *IEEE power and energy magazine, 9*(3), 62-71. [CrossRef]

[11] Jahangiri, P., & Aliprantis, D. C. (2013). Distributed Volt/VAr control by PV inverters. *IEEE Transactions on Power Systems, 28*(3), 3429-3439. [CrossRef]

[12] Tonkoski, R., Lopes, L. A., & El-Fouly, T. H. (2010). Coordinated active power curtailment of grid connected PV inverters for overvoltage prevention. *IEEE Transactions on sustainable energy, 2*(2), 139-147. [CrossRef]

[13] Brahma, S. M., & Girgis, A. A. (2004). Development of adaptive protection scheme for distribution systems with high penetration of distributed generation. *IEEE Transactions on Power Delivery, 19*(1), 56-63. [CrossRef]

[14] Photovoltaics, D. G., & Storage, E. (2018). IEEE standard for interconnection and interoperability of distributed energy resources with associated electric power systems interfaces. *IEEE std, 1547*(1547), 2018. [CrossRef]

[15] Woyte, A., Van Thong, V., Belmans, R., & Nijs, J. (2006). Voltage fluctuations on distribution level introduced by photovoltaic systems. *IEEE Transactions on energy conversion, 21*(1), 202-209. [CrossRef]

[16] Alam, M. J. E., Muttaqi, K. M., & Sutanto, D. (2013). Mitigation of rooftop solar PV impacts and evening peak support by managing available capacity of distributed energy storage systems. *IEEE transactions on power systems, 28*(4), 3874-3884. [CrossRef]

[17] Turitsyn, K., Šulc, P., Backhaus, S., & Chertkov, M. (2011). Options for control of reactive power by distributed photovoltaic generators. *Proceedings of the IEEE, 99*(6), 1063-1073. [CrossRef]

[18] Sortomme, E., Hindi, M. M., MacPherson, S. D. J., & Venkata, S. S. (2011). Coordinated charging of plug-in hybrid electric vehicles to minimize distribution system losses. *IEEE Transactions on Smart Grid, 2*(1), 198-205. [CrossRef]

[19] Umoh, V., Davidson, I., Adebiyi, A., & Ekpe, U. (2023). Methods and tools for PV and EV hosting capacity determination in low voltage distribution networks—A review. *Energies, 16*(8), 3609. [CrossRef]

[20] Zenhom, Z. M., Abdel Aleem, S. H. E., Zobaa, A. F., & Boghdady, T. A. (2024). A comprehensive review of renewables and electric vehicles hosting capacity in active distribution networks. *IEEE Access, 12*, 3672-3699. [CrossRef]

[21] Nutkani, I., Toole, H., Fernando, N., & Loh, P. C. A. (2024). Impact of EV charging on electrical distribution network and mitigating solutions - A review. *IET Smart Grid, 7*(5), 485-502. [CrossRef]

[22] Deilami, S., Masoum, A. S., Moses, P. S., & Masoum, M. A. S. (2011). Real-time coordination of plug-in electric vehicle charging in smart grids to minimize power losses and improve voltage profile. *IEEE Transactions on Smart Grid, 2*(3), 456-467. [CrossRef]

[23] Sundstrom, O., & Binding, C. (2011). Flexible charging optimization for electric vehicles considering distribution grid constraints. *IEEE Transactions on Smart Grid, 3*(1), 26-37. [CrossRef]

[24] Ma, Z., Callaway, D. S., & Hiskens, I. A. (2013). Decentralized charging control of large populations of plug-in electric vehicles. *IEEE Transactions on Control Systems Technology, 21*(1), 67-78. [CrossRef]

[25] IEEE Power and Energy Society. (2012). *IEEE guide for loading mineral-oil-immersed transformers and step-voltage regulators* (IEEE Std C57.91-2011). IEEE. [CrossRef]

[26] International Electrotechnical Commission. (2018). *Power transformers - Part 7: Loading guide for mineral-oil-immersed power transformers* (IEC 60076-7:2018). IEC. Retrieved from https://cdn.standards.iteh.ai/samples/22540/013e17b442e547a8a317649a48490f88/IEC-60076-7-2018.pdf

[27] Staszewski, L., & Rebizant, W. (2025). Quantifying overload risk: A parametric comparison of IEC 60076-7 and IEEE C57.91 standards for power transformers. *Energies, 18*(24), 6469. [CrossRef]

[28] Fernández, L. P., Román, T. G. S., Cossent, R., Domingo, C. M., & Frías, P. (2011). Assessment of the impact of plug-in electric vehicles on distribution networks. *IEEE Transactions on Power Systems, 26*(1), 206-213. [CrossRef]

[29] Kempton, W., & Tomić, J. (2005). Vehicle-to-grid power fundamentals: Calculating capacity and net revenue. *Journal of power sources, 144*(1), 268-279. [CrossRef]

[30] Oudalov, A., Cherkaoui, R., & Beguin, A. (2007, July). Sizing and optimal operation of battery energy storage system for peak shaving application. In *2007 IEEE Lausanne Power Tech* (pp. 621-625). IEEE. [CrossRef]

[31] Brooks, A., Lu, E., Reicher, D., Spirakis, C., & Weihl, B. (2010). Demand dispatch. *IEEE Power and Energy Magazine, 8*(3), 20-29. [CrossRef]

[32] Dunn, B., Kamath, H., & Tarascon, J. M. (2011). Electrical energy storage for the grid: A battery of choices. *Science, 334*(6058), 928-935. [CrossRef]

[33] Hashemi, S., & Østergaard, J. (2018). Efficient control of energy storage for increasing the PV hosting capacity of LV grids. *IEEE Transactions on Smart Grid, 9*(3), 2295-2303. [CrossRef]

[34] Navarro-Espinosa, A., & Ochoa, L. F. (2016). Probabilistic impact assessment of low carbon

technologies in LV distribution systems. *IEEE Transactions on Power Systems, 31*(3), 2192-2203. [CrossRef]

[35] Acharya, S., Dvorkin, Y., Pandžić, H., & Karri, R. (2020). Cybersecurity of smart electric vehicle charging: A power grid perspective. *IEEE Access, 8*, 214434-214453. [CrossRef]

[36] Acharya, S., Dvorkin, Y., & Karri, R. (2020). Public plug-in electric vehicles + grid data: Is a new cyberattack vector viable? *IEEE Transactions on Smart Grid, 11*(6), 5099-5113. [CrossRef]

[37] IEEE Power and Energy Society. (2022). *IEEE guide for electric power distribution reliability indices* (IEEE Std 1366-2022). IEEE. [CrossRef]

[38] Billinton, R., & Allan, R. N. (1996). *Reliability evaluation of power systems* (2nd ed.). Plenum Press. [CrossRef]

[39] Skoplaki, E., & Palyvos, J. A. (2009). On the temperature dependence of photovoltaic module electrical performance: A review of efficiency/power correlations. *Solar energy, 83*(5), 614-624. [CrossRef]

[40] Kersting, W. H. (2012). *Distribution system modeling and analysis* (3rd ed.). CRC Press. [CrossRef]

[41] Teng, J. H. (2003). A direct approach for distribution system load flow solutions. *IEEE Transactions on power delivery, 18*(3), 882-887. [CrossRef]

[42] Shirmohammadi, D., Hong, H. W., Semlyen, A., & Luo, G. X. (1988). A compensation-based power flow method for weakly meshed distribution and transmission networks. *IEEE Transactions on Power Systems, 3*(2), 753-762. [CrossRef]

[43] European Committee for Electrotechnical Standardization. (2022). *Voltage characteristics of electricity supplied by public electricity networks* (EN 50160:2022). CENELEC. Retrieved from https://standards.iteh.ai/catalog/standards/clc/083c552d-f4b8-4373-a5ec-8a27b6c8d37d/en-50160-2022?srsltid=AYCX9vKpWr5bE8Lc_88SUn1jQx5sdFn3k3N2O6b95NUDvvABNbjR8kuA

[44] Stepka, E. (2020, October 26). *ANSI C84.1-2020: Electric power systems voltage ratings (60 Hz)*. The ANSI Blog. Retrieved from https://blog.ansi.org/ansi/ansi-c84-1-2020-electric-voltage-ratings-60-hz/

Appendix A. Voltage-magnitude change across a short radial line segment

This appendix derives the approximation of Eq. (15). Consider a short segment of the radial feeder between a sending node s and a receiving node r, with series impedance $Z = R + jX$ and negligible shunt admittance. Let $S_r = P + jQ$ be the complex power drawn at the receiving end, with P and Q positive when power flows toward node r and is consumed there (as in Section 2.4) and negative for generation exported at r. Taking the receiving-end voltage V_r as the phase reference, the segment current and the sending-end voltage are

$$I = \left(\frac{S_r}{V_r}\right)^* = \frac{P - jQ}{V_r} \tag{A1}$$

$$V_s = V_r + Z\,I = V_r + \frac{(R + jX)(P - jQ)}{V_r} \tag{A2}$$

With $a = (RP + XQ)/V_r$ and $b = (XP - RQ)/V_r$, the real and imaginary parts of Eq. (A2) give

$$V_s = (V_r + a) + j\,b \tag{A3}$$

The voltage-magnitude drop across the segment, $\Delta V = |V_s| - V_r$, is therefore

$$\Delta V = \sqrt{(V_r + a)^2 + b^2} - V_r \approx a + \frac{b^2}{2\,(V_r + a)} \tag{A4}$$

where the approximation is the first-order expansion of the square root for $b \ll V_r + a$. In distribution feeders the voltage drop over one segment is a small fraction of the nominal voltage ($a \ll V_r$) and the phase-angle difference between the two ends is small ($b \ll V_r$), so the second term of Eq. (A4) is of second order. For illustration, $a = 0.05$ p.u. and $b = 0.02$ p.u. give a neglected term of about 2×10^{-4} p.u., which is 0.4% of a. Retaining only the first term and writing V for the receiving-end voltage gives Eq. (15), $\Delta V \approx (RP + XQ)/V$.

For a balanced three-phase feeder with per-phase resistance R and reactance X, total three-phase powers P and Q and line-to-line voltage V_{LL}, the factors of $\sqrt{3}$ in the phase voltage and in the phase power cancel, and the same expression holds for the line-to-line voltage:

$$\Delta V_{LL} \approx \frac{RP + XQ}{V_{LL}} \tag{A5}$$

In per-unit quantities with $V \approx 1$ p.u., the expression reduces to $\Delta V \approx RP + XQ$.

A positive ΔV is a voltage drop from s to r, and a negative ΔV is a voltage rise at r. Under load ($P > 0, Q > 0$) the voltage falls along the feeder. For PV export, $P = -P_{PV}$, and with inverter reactive-power absorption $Q = +|Q_{inv}|$ the expression becomes $\Delta V \approx (-RP_{PV} + X|Q_{inv}|)/V$, which is the form used in Section 2.5. The resistive term dominates when $R/X > 1$, as in the case-study feeder ($R/X \approx 1.15$); this explains why active-power export raises the voltage and why reactive-power absorption can offset only part of the rise. For a node k reached through several segments, the voltage drop is approximately the sum of the segment drops,

$$\Delta V_k \approx \sum_{l \in \mathrm{path}(k)} \frac{R_l P_l + X_l Q_l}{V_l} \tag{A6}$$

where $\mathrm{path}(k)$ is the set of segments between the source and node k, and P_l and Q_l are the total active and reactive power flowing through segment l toward the nodes downstream of it. Equations (15) and (A6) are used for interpretation only: all voltages reported in Section 5 are obtained from the BFS solution of Section 2.4, which retains the neglected quadrature term and the feeder losses.

Appendix B. State of charge of the EV batteries and the BESS

The state of charge (SoC) of a battery is the energy stored in it expressed as a fraction of its usable energy capacity E (kWh):

$$\mathrm{SoC}(t) = \frac{E_{stored}(t)}{E}, \quad 0 \le \mathrm{SoC}(t) \le 1 \tag{A7}$$

SoC is therefore dimensionless (multiplied by 100 for a percentage). The usable capacity is 60 kWh for the vehicles and 200 kWh for the BESS in the case study (Table 1).

Let $P_{ch} \geq 0$ be the power drawn from the grid by the charger and $P_{dis} \geq 0$ the power delivered to the grid by the discharging battery ($P_{EV,i}$ and $P_{V2G,i}$ for vehicle i). With charging efficiency η_c and discharging efficiency η_d, the power entering the battery during charging is $\eta_c P_{ch}$, and the power leaving the battery during discharge is P_{dis}/η_d. The state of charge therefore obeys

$$E \frac{d\,\mathrm{SoC}(t)}{dt} = \eta_c P_{ch}(t) - \frac{P_{dis}(t)}{\eta_d} \tag{A8}$$

which combines Eqs. (1) and (29); charging and discharging are mutually exclusive, Eqs. (30) and (31). For the simulation time step Δt (15 min, Table 1), with the powers constant within the step, the update is

$$\mathrm{SoC}(t + \Delta t) = \mathrm{SoC}(t) + \frac{[\eta_c P_{ch}(t) - P_{dis}(t)/\eta_d]\,\Delta t}{E} \tag{A9}$$

For an EV, the daily energy requirement E_d of Section 2.2 is taken as the energy to be added to the battery during the stay, so the states of charge at arrival and at the required departure are related by

$$\mathrm{SoC}_{dep,i} = \mathrm{SoC}_{arr,i} + \frac{E_{d,i}}{E_i} \tag{A10}$$

and the energy that the charger draws from the grid is E_d/η_c. The departure requirement of Eq. (28) can be met only if the vehicle remains connected long enough at the maximum charging power, that is,

$$\eta_c P_{EV,\max,i}\,(T_{dep,i} - t_{arr,i}) \geq E_{d,i} \tag{A11}$$

where $t_{arr,i}$ is the arrival time. With $P_{EV,\max} = 7.2$ kW and $\eta_c = 0.95$ (Table 1), the median requirement of 27 kWh needs about $27/(0.95 \times 7.2) \approx 3.9$ h of charging, which fits within the interval between an arrival time between 17:00 and 22:00 and the departure at 07:00. The requirement must also respect the SoC window of Eq. (27): $E_{d,i}$ cannot exceed $E_i(\mathrm{SoC}_{\max,i} - \mathrm{SoC}_{\min,i})$, which is 51 kWh for the values of Table 1, so that sampled values above this limit have to be truncated.

For V2G, the energy that a connected vehicle can still deliver to the grid at time t is bounded by the V2G floor,

$$E_{V2G,avail,i}(t) = \eta_d E_i\,[\mathrm{SoC}_i(t) - \mathrm{SoC}_{V2G,\min,i}] \tag{A12}$$

and the floor must be high enough that charging at the maximum power during the remaining time still satisfies Eq. (28). A floor that guarantees this at every time is

$$\mathrm{SoC}_{V2G,\min,i}(t) = \max\Big\{\mathrm{SoC}_{\min,i},\ \mathrm{SoC}_{dep,i} - \frac{\eta_c P_{EV,\max,i}\,(T_{dep,i} - t)}{E_i}\Big\} \tag{A13}$$

Eq. (A11) is a feasibility check on the stay of the vehicle. Its left-hand side is the largest energy that the charger puts in the battery between the arrival time $t_{arr,i}$ and the required departure time $T_{dep,i}$, when it charges at the maximum power $P_{EV,\max,i}$ with efficiency η_c; the right-hand side is the energy requirement $E_{d,i}$. If the inequality holds, the departure requirement of Eq. (28) is met.

Eq. (A12) provides the energy that a connected vehicle can still deliver to the grid at time t. The term $E_i(\mathrm{SoC}_i(t) - \mathrm{SoC}_{V2G,\min,i})$ is the energy stored in the battery above the V2G floor, and it is multiplied by the discharging efficiency η_d because, according to Eq. (A8), only the fraction η_d of the energy taken out of the battery reaches the grid. If the state of charge is at or below the floor, the available energy is zero. The dispatch rule of Section 3.4(c) allocates the required discharge to the vehicles in proportion to this quantity. For example, a 60-kWh vehicle at $\mathrm{SoC} = 0.80$ with a floor of 0.30 can deliver $0.95 \times 60 \times (0.80 - 0.30) = 28.5$ kWh.

Eq. (A13) defines the V2G floor itself. It is the larger of two values: the lower limit $\mathrm{SoC}_{\min,i}$ of Eq. (27), and the state of charge from which charging at full power during the remaining time $T_{dep,i} - t$ just reaches the required

state of charge at departure, $\mathrm{SoC}_{dep,i} - \eta_c P_{EV,\max,i}(T_{dep,i} - t)/E_i$. The vehicle can therefore be discharged down to this level and still be recharged before it leaves. Early in the evening the remaining time is long, the second value is small or negative, and the floor equals $\mathrm{SoC}_{\min,i}$; it rises as the departure approaches. As an illustration, take a vehicle that arrives with $\mathrm{SoC} = 0.20$ and needs 27 kWh, so that $\mathrm{SoC}_{dep,i} = 0.20 + 27/60 = 0.65$. At 20:00, 11 h before departure, the second value is $0.65 - 0.95 \times 7.2 \times 11/60 \approx -0.60$, so the floor is $\mathrm{SoC}_{\min,i} = 0.10$. The second value exceeds 0.10 only during the last $(0.65 - 0.10) \times 60/(0.95 \times 7.2) \approx 4.8$ h before departure, that is, after about 02:10. The V2G floor of 0.30 in Table 1 is higher than this value throughout the dispatch window of 18:00-20:00, and the departure requirement is therefore not endangered by V2G discharge.

The feeder BESS follows Eqs. (A7)-(A9) with $E = 200$ kWh and the SoC limits of Eq. (38); the only difference from a vehicle is that its charging and discharging powers are set by the dispatch rule of Section 3.4 and not by a departure requirement.

Appendix C. Hosting capacity: scope and screening estimates

Hosting capacity is not a single property of a feeder: it depends on the performance indices chosen, on the limits applied to them, on the load and generation profiles and on the control capabilities available [19, 20]. In this paper the limiting phenomena are overvoltage and undervoltage (Eq. (34)), thermal loading of the lines and of the transformer (Eqs. (35) and (36)), the inverter capability (Eq. (37)) and the storage state of charge (Eq. (38)); protection coordination, harmonics and flicker are not evaluated. The hosting capacities of Section 5.5 are obtained from the simulation-based search of Section 3.5. Two first-order relations that can be used for screening, and for checking the order of magnitude of the simulated values, are given below; they do not replace the time-series solution.

Voltage-rise limit for PV. Let V_0 be the voltage at a node, at the time considered, without PV; let R_{eq} and X_{eq} be the equivalent series resistance and reactance between the source and the node (weighted by the position of the PV systems when they are distributed along the feeder); and let $Q_{abs} = P_{PV} \tan \varphi_{inv}$ be the reactive power absorbed by the inverters, with φ_{inv} the inverter power-factor angle, limited by Eq. (18). From Eq. (15), the upper voltage limit is respected if

$$V_0 + \frac{R_{eq} P_{PV} - X_{eq} Q_{abs}}{V} \leq V_{\max} \tag{A14}$$

which gives the maximum PV active power at that node,

$$P_{PV,\max} \approx \frac{V\,(V_{\max} - V_0)}{R_{eq} - X_{eq} \tan \varphi_{inv}} \tag{A15}$$

valid when $R_{eq} > X_{eq} \tan \varphi_{inv}$. For unity power factor, Eq. (A15) reduces to $P_{PV,\max} \approx V(V_{\max} - V_0)/R_{eq}$, and reactive-power absorption increases the permissible PV power by the factor $1/(1 - (X_{eq}/R_{eq}) \tan \varphi_{inv})$. The installed PV capacity follows from $P_{PV,\max}$ and the PV output at the time of the maximum voltage.

Transformer-loading limit for EVs. Let S_{rated} be the transformer rating, and $P_{base,pk}$ and Q_{pk} the base-load active and reactive power at the evening peak (the chargers are assumed to operate at unity power factor). Requiring $K(t) \leq 1$ (Eq. (36)) at that time, with the coincident EV demand of Eq. (5), gives the maximum number of EVs

$$N_{EV,\max} \approx D_f \frac{\sqrt{S_{rated}^2 - Q_{pk}^2} - P_{base,pk}}{P_{EV,rated}} \tag{A16}$$

where $P_{EV,rated}$ is the charger rating, and the EV hosting capacity as a share of customers is $N_{EV,\max}$ divided by the number of customers (120 in the case study). As stated in Section 2.2, the diversity factor D_f belongs to screening calculations and is not combined with time-series profiles, in which the coincidence is already represented.

Sampling error of the violation probability. Equation (39) is a binomial proportion estimated from N_{MC} samples, so its standard error is

$$SE\,(P_{viol}) = \sqrt{\frac{P_{viol}\,(1 - P_{viol})}{N_{MC}}} \tag{A17}$$

At the acceptance value $\varepsilon_v = 0.05$, a standard error of 0.01 requires $N_{MC} \approx \varepsilon_v(1-\varepsilon_v)/0.01^2 \approx 475$ samples. The number of samples must therefore be large enough for the decision $P_{viol} \leq \varepsilon_v$ not to be dominated by sampling noise. With the $N_{MC} = 120$ samples used in this study (Table 1), the standard error at $P_{viol} = 0.05$ is about 0.02, so levels whose violation probability lies close to ε_v may be accepted or rejected by chance, and the reported hosting capacities carry an uncertainty of about one search step.

Appendix D. Backward/forward-sweep load flow

This appendix describes the load-flow solution referred to in Section 2.4. It is a nonlinear AC power flow for a balanced radial network, solved in per unit on the base voltage of the 0.4 kV secondary feeder (single-phase equivalent), and not a linearised model. The source is the ideal 1.00 p.u. voltage at the secondary busbar of the transformer. Every bus k other than the source has exactly one upstream neighbour j and one connecting section l, so the network has no loops and Eqs. (12) and (13) can be evaluated without factorising a bus admittance matrix. For each time step t the procedure is as follows.

1. Initialisation: set $V_k = 1.00\angle 0^\circ$ p.u. at all buses and $Q_{inv,k} = 0$.
2. Bus powers: compute the net complex power $S_k(t)$ of each bus from Eq. (11), using the base load, EV, V2G and PV values of the time step and the latest value of $Q_{inv,k}$.
3. Backward sweep: starting from the buses at the ends of the feeder and moving toward the source, compute the section currents $I_l(t)$ from Eq. (12); the current of a section is the current drawn at its receiving bus plus the currents of the sections downstream of it.
4. Forward sweep: set the source voltage to 1.00 p.u. and, moving away from the source, update the bus voltages from Eq. (13).
5. Volt/VAr update: evaluate $Q_{inv,k}$ from the characteristic of Eq. (17) at the new bus voltages, limited by Eqs. (16) and (18), with active-power curtailment under reactive-power priority when the capability limit is reached (Section 2.5).
6. Convergence: stop if the criterion of Eq. (14) is satisfied with $\varepsilon = 10^{-6}$ p.u. (Table 1); otherwise return to step 2.
7. Outputs: the bus voltages $V_k(t)$, the section apparent power and loading, the feeder loss $P_{loss}(t) = \sum \mathrm{Re}(Z_l)|I_l(t)|^2$, and the transformer loading $K(t)$ of Eq. (20), obtained from the apparent power $S_{load}(t)$ at the secondary busbar.

A linearised alternative is obtained by neglecting the losses and the quadrature component of the voltage drop (Appendix A) and assuming voltages close to 1 p.u., which reduces the sweeps to the linearised DistFlow relation

$$V_k^2 \approx V_j^2 - 2\,(R_l P_l + X_l Q_l) \tag{A18}$$

Because $V_j^2 - V_k^2 = (V_j - V_k)(V_j + V_k) \approx 2V\Delta V$, Eq. (A18) is equivalent to Eq. (15) for $V \approx 1$ p.u. It is the type of relation used to express the network constraints linearly in the coordinated-charging problem of Section 3.3.

Appendix E. Objective functions

Scheduling objective of Eq. (25). The three terms of Eq. (25) have different units: the peak demand $\max P_{grid}(t)$ is a power (kW), the loss term $\sum P_{loss}(t)\Delta t$ is an energy (kWh) and the cost term $\sum C(t)P_{grid}(t)\Delta t$ is a monetary amount ($). A dimensionless form is obtained by normalising each term by its value in the unmanaged case (the reference values P_{peak}^{ref}, E_{loss}^{ref} and C^{ref}):

$$J = w_1 \frac{\max_t P_{grid}(t)}{P_{peak}^{ref}} + w_2 \frac{\sum_t P_{loss}(t)\,\Delta t}{E_{loss}^{ref}} + w_3 \frac{\sum_t C(t)\,P_{grid}(t)\,\Delta t}{C^{ref}}, \quad w_1 + w_2 + w_3 = 1 \tag{A19}$$

The weights w_1, w_2 and w_3 set the relative priority of peak reduction, loss reduction and charging cost. In the coordinated charging of Section 3.3 the peak term carries the dominant weight, so that the aggregator first

flattens the feeder demand and uses the loss and cost terms to choose among schedules with the same peak. The maximum is handled with the auxiliary variable $P_{peak} \geq P_{grid}(t)$ for all t, and P_{peak} replaces $\max P_{grid}(t)$ in Eq. (A19). The complete scheduling problem is to minimise J over the charging powers $P_{EV,i}(t)$ (and, where V2G is allowed, $P_{V2G,i}(t)$) subject to the charger limit of Eq. (26), the state-of-charge window of Eq. (27), the departure requirement of Eq. (28), the V2G constraints of Eqs. (29)-(31), the power balance of Eq. (32a) or (32b) and the network constraints of Eqs. (34)-(36).

Hosting-capacity objective of Eq. (33). When EV and PV hosting capacity are maximised together, the two objectives can be combined by a weighted sum,

$$\max \; w_{EV} H_{EV} + w_{PV} H_{PV}, \;\; w_{EV} + w_{PV} = 1, \; w_{EV}, w_{PV} \geq 0 \tag{A20}$$

or the Pareto front can be traced by maximising one of them while the other is held at a given level H^0, for example

$$\max \; H_{EV} \quad \text{subject to} \quad H_{PV} \geq H_{PV}^0 \tag{A21}$$

subject to the constraints of Eqs. (34)-(38). The second form is the one used in this paper: H_{EV} is evaluated with the PV share held at its base value and H_{PV} with the EV share held at its base value (Section 3.5). Because the constraints are nonlinear and the EV and PV profiles are stochastic, the maximisation is carried out by the incremental search of Eqs. (39)-(40) and not by an optimisation solver: the hosting capacity is the largest penetration level (the highest step of the incremental search, in percentage points of customers with EV chargers or rooftop PV, reached before the first violation) whose violation probability does not exceed ε_v.



Rupali Brahmachary was born in India, in 1997. She received her B.Tech. degree in Electrical Engineering from Techno India University, West Bengal, in 2018, and her M.Tech. degree in Power Systems Engineering from the National Institute of Technology Nagaland in 2020. She received her Ph.D. degree from the National Institute of Technology Durgapur in 2026. Her main research interests include electric vehicles, demand-side management, distribution network planning and optimization, machine learning-based load forecasting, power quality, and renewable energy integration. She is currently working as a Project Associate-II in the Department of Electrical Engineering, National Institute of Technology Durgapur, India. (Email: brahmachary.rupali29@gmail.com)



Ahmet Teke is a professor in the Department of Electrical and Electronics Engineering at Çukurova University. Having completed his Bachelor's, Master's, and Ph.D. degrees at Çukurova University, Prof. Teke has conducted extensive research throughout his academic career in the areas of power electronics, power quality, renewable energy integration, smart grids, power converters and electric vehicle charging technologies. He has authored numerous national and international journal articles, conference papers, and funded research projects. In addition to teaching undergraduate and graduate courses, he actively participates in university-industry collaboration projects focused on renewable energy and power systems. (Email: ahmetteke@cu.edu.tr)



Aleksa Babic was born in Belgrade, Serbia, in 1978. As an adolescent he moved to the USA with his parents. He graduated from the Faculty of Electrical Engineering, University of Minnesota, Twin Cities, in 2003. He received his M.Sc. degree in 2007 from the University of Minnesota, Twin Cities, MN, where he worked at the time as a research assistant. He received his doctorate from the Faculty of Electrical Engineering, University of Kragujevac, in 2014 while working full time as engineering support for energy traders at Southern California Edison, Rosemead, CA. His main research interests include power flow, optimal power flow, loss allocation, locational marginal price decomposition, and optimization in power system operations and planning. He currently works full time as an electrical engineer in the Operations Engineering Group at Western Area Power Administration in Phoenix, AZ. (Email: babic@wapa.gov)



Zoran Miljanić was born in Montenegro, in 1980. He graduated from the Faculty of Electrical Engineering, University of Montenegro, in 2002. He received his M.Sc. and Ph.D. degrees in 2006 and 2013, respectively, from the Faculty of Electrical Engineering, University of Montenegro. His main research interests include the analysis and control of power systems, planning and organization of the power sector, energy efficiency, the environmental impacts of the power sector, metaheuristics and optimization methods. He is currently an Associate Professor with the Faculty of Electrical Engineering, University of Montenegro, and an R&D engineer at Refleksing LLC, Podgorica, Montenegro. (Email: zormi@ac.me)